

Inverse Gertsenshtein effect as a probe of high-frequency gravitational waves

Yutong He,^{a,b} Sambit K. Giri,^b Ramkishor Sharma,^b
Salome Mtchedlidze^{c,d} and Ivelin Georgiev^a

^aThe Oskar Klein Centre, Department of Astronomy, Stockholm University, AlbaNova, SE-10691 Stockholm, Sweden

^bNordita, KTH Royal Institute of Technology and Stockholm University, Hannes Alfvéns väg 12, SE-10691 Stockholm, Sweden

^cDipartimento di Fisica e Astronomia, Università di Bologna, via Gobetti 93/2, 40122 Bologna, Italy

^dSchool of Natural Sciences and Medicine, Ilia State University, 3-5 Cholokashvili Ave, Tbilisi, GE-0194, Georgia

April 25, 2024

E-mail: yutong.he@su.se, sambit.giri@su.se, ramkishor.sharma@su.se,
salome.mtchedlidze@unibo.it, ivelin.georgiev@astro.su.se

Abstract. We apply the inverse Gertsenshtein effect, i.e., the graviton-photon conversion in the presence of a magnetic field, to constrain high-frequency gravitational waves (HFGWs). Using existing astrophysical measurements, we compute upper limits on the GW energy densities Ω_{GW} at 16 different frequency bands. Given the observed magnetisation of galaxy clusters with field strength $B \sim \mu\text{G}$ correlated on $\mathcal{O}(10)$ kpc scales, we estimate HFGW constraints in the $\mathcal{O}(10^2)$ GHz regime to be $\Omega_{\text{GW}} \lesssim 10^{16}$ with the temperature measurements of the Atacama Cosmology Telescope (ACT). Similarly, we conservatively obtain $\Omega_{\text{GW}} \lesssim 10^{13}(10^{11})$ in the $\mathcal{O}(10^2)$ MHz ($\mathcal{O}(10)$ GHz) regime by assuming uniform magnetic field with strength $B \sim 0.1$ nG and saturating the excess signal over the Cosmic Microwave Background (CMB) reported by radio telescopes such as the Experiment to Detect the Global EoR Signature (EDGES), LOw Frequency ARray (LOFAR), and Murchison Widefield Array (MWA), and the balloon-borne second generation Absolute Radiometer for Cosmology, Astrophysics, and Diffuse Emission (ARCADE2) with graviton-induced photons. The upcoming Square Kilometer Array (SKA) can tighten these constraints by roughly 10 orders of magnitude, which will be a step closer to reaching the critical value of $\Omega_{\text{GW}} = 1$ or the Big Bang Nucleosynthesis (BBN) bound of $\Omega_{\text{GW}} \simeq 1.2 \times 10^{-6}$. We point to future improvement of the SKA forecast and estimate that proposed CMB measurement at the level of $\mathcal{O}(10^{0-2})$ nK, such as Primordial Inflation Explorer (PIXIE) and Voyage 2050, are needed to viably detect stochastic backgrounds of HFGWs.

Contents

1	Introduction	1
2	Graviton-photon conversion	3
2.1	Galaxy clusters	3
2.2	Cosmological scales	4
2.3	Impact on the blackbody CMB radiation	5
3	Existing measurements	6
3.1	Kinematic Sunyaev-Zel'dovich effect	6
3.2	Excess radio background	8
4	Future surveys	10
4.1	Forecast with the SKA	10
4.2	Forecast with future CMB surveys	12
5	Discussions	12
5.1	Sensitivity comparison	13
5.2	Alternative methods to probe HFGW	14
6	Conclusion	15
A	Inverse Gertsenshtein formalism	15
B	Modelling baryonic physics inside galaxy clusters	19
C	Full posterior distribution of the SKA forecast study	19

1 Introduction

Gravitational waves (GWs) are a unique cosmic messenger as they propagate across vast distances unimpeded by the cosmic medium. Astrophysical GW signals from binary mergers have been observed in the frequency (f) band from few Hz to kHz by LIGO-Virgo-KAGRA (LVK) [1–3], while a stochastic GW background (SGWB) in the nHz range has recently been discovered by pulsar timing arrays (PTAs) [4–7]. On the largest scales, corresponding to e.g., $f \lesssim 10^{-11}$ Hz, the cosmic microwave background (CMB) also constrains primordial SGWB in terms of the measured tensor-to-scalar ratio [8–11]. With the upcoming space-based interferometers such as LISA [12], the mHz range will also be extensively studied. On the other hand, the high-frequency regime, broadly defined to be above kHz, is relatively less explored. However, given that the high-frequency GWs (HFGWs) could potentially be sourced by new physics both in the early and late Universe — including but not limited to certain types of inflation [13–16], preheating and reheating [17, 18], beyond-Standard Model phase transitions (see Refs. [19, 20] and the discussions therein), black hole (BH) superradiance [21], and light primordial black holes (PBH) [22–29] — it is important to explore GWs in the MHz, GHz, or even higher frequency ranges [20].

To circumvent the lack of dedicated HFGW detectors, many indirect searches are proposed. A novel approach relies on the inverse Gertsenshtein effect [24, 30–36], which describes the conversion of gravitons into photons of the same frequency in the presence of a magnetic field [37, 38]. The effect is typically studied in two distinct contexts:

- (i) Astrophysical and cosmological magnetic fields: Magnetic fields are ubiquitous as they are observed across many scales in the Universe, from planets and stars [39–41] to galaxy and cluster scales [42, 43]. Correspondingly, graviton-photon conversion is studied in the presence of planetary magnetospheres [44], highly magnetised objects such as neutron stars, pulsars, magnetars, and BHs [45–49], Milky Way magnetic fields [50] and large-scale magnetic fields originating in the early Universe, i.e., primordial (cosmological) magnetic fields (PMFs) [33, 51, 52].
- (ii) Laboratory settings: Although experiments specifically dedicated to inverse Gertsenshtein effect are yet to be conducted, existing instruments that involve controlled magnetic fields and electromagnetic (EM) sensors, such as axion detectors, can be repurposed and their results reinterpreted as upper limits on HFGWs [53–63].

In this work, we mainly focus on the former approach but also briefly mention the latter method. Specifically in terms of approach (i), we introduce the measurement of the kinematic Sunyaev-Zeldovich (kSZ) effect in galaxy clusters as a novel method for detecting HFGWs. This effect originates from the amplification of CMB photon energy through inverse Compton scattering by the high-energy electrons within these clusters (see Ref. [64] for a review). However, the induced Gertsenshtein photons due to gravitons passing through galaxy cluster magnetic fields can also contribute to the increase of photon energy usually interpreted as the kSZ effect. We place conservative limits on HFGWs within the frequency range of $\mathcal{O}(10^2)$ GHz using the most recent observations conducted by the Atacama Cosmology Telescope (ACT) [65, 66].

We expand the study of approach (i) by examining the impact of the inverse Gertsenshtein effect on the radio background against which the cosmological 21-cm signal is measured. This signal arises from the hyperfine splitting of ground-state neutral hydrogen atoms in the intergalactic medium (IGM) during cosmic dawn and the epoch of reionisation, corresponding to the period when the first light sources formed and reionised IGM gas (see Ref. [67] for a review). Previous studies have hinted at the presence of excess radio photons beyond the blackbody CMB [68, 69] to explain the 21-cm signal measurements [70]. Despite several proposed explanations for its physical origins, including BHs [71] and radio galaxies [72] at high redshift, this phenomenon remains uncertain. In this study, we investigate photons produced by the inverse Gertsenshtein effect as a potential source of this excess radio background. Currently, several ongoing efforts, such as the Experiment to Detect the Global EoR Signature (EDGES) [70], LOw-Frequency ARray (LOFAR) [73], and Murchison Widefield Array (MWA) [74] are improving the measurements of the 21-cm signal during these early epochs. And the balloon-borne second generation Absolute Radiometer for Cosmology, Astrophysics, and Diffuse Emission (ARCADE2) has also detected a radio excess beyond the 21-cm frequency. We place upper limits on the HFGWs by conservatively assuming that they induce photons that saturate all of the reported radio excess over CMB. In the near future, significant improvements in these measurements are expected, primarily driven by the Square Kilometre Array (SKA) [75]. These advancements will lead to improved constraints on the astrophysical processes governing the formation of first-generation light sources [76, 77], the

properties of reionisation [78], and cosmological aspects [79, 80]. We forecast the potential of the SKA in indirectly constraining the HFGWs. By comparing the upper limit constraints derived using existing measurements, forecast using SKA, and estimated using proposed future CMB surveys, we note the general status of HFGW detection proposals and future work to improve them.

The paper is structured as follows. In Section 2, we present the result of the graviton-photon conversion in the classical limit, given the context of the large-scale magnetisation of the Universe. The detailed formulation of the effect can be found in appendix A. In Section 3, we present conservative upper bounds on HFGWs obtained from the kSZ observations with the ACT (Section 3.1), and from the reported excess radio background by EDGES, LOFAR, MWA, and ARCADE2 (Section 3.2). In Section 4, we present forecast constraints from SKA (Section 4.1) and future CMB surveys (Section 4.2). We discuss the findings in Section 5 and conclude in Section 6.

Unless otherwise stated, we set $c = \hbar = k_B = \varepsilon_0 = 1$, adopt the metric signature $(-+++)$, and the gravitational coupling $\kappa \equiv 8\pi G_N/c^4$, with G_N being Newton’s constant. We assume the standard Λ CDM cosmology parameters [10]: matter parameter $\Omega_m = 0.31$, baryon parameter $\Omega_b = 0.049$, dark energy parameter $\Omega_\Lambda \simeq 1 - \Omega_m$, Hubble constant $H_0(100h) = 67$ km/(Mpc·s), and the blackbody CMB temperature $T_{\text{CMB}} \simeq 2.725$ K.

2 Graviton-photon conversion

We will describe the theory behind the conversion of gravitons to photons at galaxy cluster and cosmological scales in Section 2.1 and 2.2 respectively. In Section 2.3, we will discuss the implications of such conversions on the CMB.

2.1 Galaxy clusters

We briefly discuss here the framework in which gravitons are converted into photons. GWs with frequency f traversing through a galaxy-cluster magnetic field with amplitude B and coherent scale (or equivalently correlation length) l_{cor} ¹ can be converted into photons of the same frequency with a small but nonzero probability $\mathcal{P}_{g \rightarrow \gamma}$ (see appendix A for the detailed derivation)

$$\mathcal{P}_{g \rightarrow \gamma} \approx 5.87 \times 10^{-29} \left(\frac{B}{1 \mu\text{G}} \right)^2 \left(\frac{f}{100 \text{ GHz}} \right)^2 \left(\frac{10^{-3} \text{ cm}^{-3}}{n_e} \right)^2 \left(\frac{D}{1 \text{ Mpc}} \right) \left(\frac{10 \text{ kpc}}{l_{\text{cor}}} \right), \quad (2.1)$$

where n_e is the electron density of the medium, and D is the total travel distance of GWs. We assume $D > l_{\text{cor}}$ and a constant field strength within the coherence scale of the magnetic field. Equation (2.1) shows that the conversion probability depends on the strength and structure of the magnetic field. Both strong ($B > 1 \mu\text{G}$ [81–84]) and weaker fields ($B \lesssim 0.1 - 1 \mu\text{G}$ [85, 86]) have been observed to be correlated over scales of $\mathcal{O}(10)$ kpc in galaxy clusters and in the dilute plasma between galaxies, known as the intracluster medium (ICM) (see Refs. [87, 88] for reviews). These are obtained using various methods such as Faraday rotation measurements [89, 90] or the equipartition hypothesis for the observed cluster-scale,

¹Note that we directly take the observationally inferred values of l_{cor} here. In numerical simulations with a known magnetic field energy spectrum $E_B(k)$ in wavenumber k space, the correlation length l_{cor} is instead computed via the expression $l_{\text{cor}} = \int_0^\infty dk k^{-1} E_B(k) / \int_0^\infty E_B(k) dk$.

diffuse synchrotron emission [91, 92]². The origin of such large-scale correlated magnetic fields is debated. A commonly accepted hypothesis is that they result from the amplification of weak seed fields, which could originate either in the early Universe, referred to as PMFs, or at later epochs, e.g., during reionisation and structure formation.

The cosmological magnetohydrodynamic (MHD) simulations, which account for the amplification of weak seed magnetic fields through the combined effects of gravitational collapse and small-scale dynamos [97–101], reproduce ICM magnetic fields with $B \sim 1 \mu\text{G}$ strengths (see Ref. [102] for a review). However, the obtained strength as well as the coherence scale of the magnetic field at the current epoch depend on the magnetogenesis scenarios, and on the evolution of the field in the pre- and post-recombination epochs. For instance, in the case of PMFs, the correlation lengths of the field can be as large as 230 – 400 kpc at $z = 0$ [101]. The observational constraints are also affected by the assumption of the field topology [82, 103–105]. Therefore, the precise calculation of the inverse Gertsenshtein effect depends on our understanding of the magnetic field structure and strength on the relevant scales. Having this caveat in mind, we explore in our work the conversion of gravitons into photons on cluster scales (Section 3.1), setting $B \sim 0.1 \mu\text{G}$ over $l_{\text{cor}} \sim 10 \text{ kpc}$.

2.2 Cosmological scales

Beyond the scales of galaxies and clusters, redshift dependence of the electron distribution becomes important when considering inverse Gertsenshtein effect across cosmological epochs. The graviton-photon conversion probability modifies to [52]

$$\mathcal{P}_{g \rightarrow \gamma} \approx 3.78 \times 10^{-20} \left(\frac{B}{0.1 \text{ nG}} \right)^2 \left(\frac{f}{f_{\text{eq}}} \right)^2 \left(\frac{1 \text{ Mpc}}{\Delta l_0} \right) \left(\frac{\mathcal{I}(z_{\text{ini}})}{6 \times 10^6} \right), \quad (2.2)$$

where $f_{\text{eq}} = k_{\text{B}} T_{\text{CMB}} / (2\pi\hbar) \approx 56.79 \text{ GHz}$ is the characteristic frequency of CMB assumed to be in equilibrium, $\Delta l_0 = \min(l_{\text{eq}}, l_{\text{cor}}^0)$ with $l_{\text{eq}} \approx 95 \text{ Mpc}$ being the comoving scale of the scalar mode entering the horizon at radiation-matter equality, and l_{cor}^0 being the present-day coherence length of the magnetic field, and $\mathcal{I}(z_{\text{ini}})$ is an integral determined by the ionisation fraction $X_e(z)$ [106]

$$\mathcal{I}(z_{\text{ini}}) = \int_{z_{\text{obs}}}^{z_{\text{ini}}} dz (1+z)^{-3/2} X_e^{-2}(z), \quad (2.3)$$

where z_{obs} is the redshift at which observations are made. In line with the assumptions made in Ref. [52], we consider graviton-photon conversion taking place post-CMB and therefore take $z_{\text{ini}} \sim 1100$ in equation (2.3) (see Ref. [107] for a study of pre-CMB conversion).

We note that contrary to the case discussed in Section 2.1, here we specifically assume the primordial origin of the observed large-scale magnetic fields. Although the current radio telescopes detect the diffuse radio emission only up to a redshift of $z \sim 0.9$ [108–110], the analysis of the distant blazar spectra by the Fermi-LAT and High Energy Stereoscopic System (H.E.S.S.) collaborations [111] hints at the existence of Mpc-correlated, volume-filling magnetic fields in the IGM. This favours primordial magnetogenesis scenarios in the inflationary [112–116] or phase-transitional [117–120] epochs.

²The Faraday rotation effect refers to the change of the intrinsic polarisation plane of the polarised emission as the light passes through the magnetised medium, and is widely used for inferring the magnetic field strength and structure both on galaxy cluster scales and in the rarefied cosmic regions [93, 94]. The synchrotron emission, observed in the radio waveband, traces cluster magnetic fields as well as magnetic fields extending beyond galaxy clusters [95, 96].

Uncertainties, again, remain in the understanding of the evolution of PMFs across different cosmological epochs (see Ref. [121] for a review). In this work, to analyse HFGWs on cosmological scales (Section 3.2), we choose the field properties normalised in equation (2.2), i.e., $B \sim 0.1$ nG and $l_{\text{cor}} \sim 1$ Mpc, which yield considerably higher conversion probability than in individual local structures such as galaxies or clusters shown in equation (2.1). We justify the choice of the field strength $B \sim 0.1$ nG by noting that although it is orders of magnitude higher than the lower bounds derived from the blazar spectra observations, i.e., $B > 10^{-14}$ G in voids [111], it is well within the derived values of $B < 40$ nG [93] and $B < 4$ nG [94] in the IGM, and $30 \leq B \leq 60$ nG for filaments [122]. In our future work we will take into account magnetic field characteristics in different epochs predicted or modelled by MHD simulations, i.e., weighting the integral in equation (2.2) by the corresponding field strength and coherence scales.

2.3 Impact on the blackbody CMB radiation

With a small but non-vanishing conversion probability $\mathcal{P}_{g \rightarrow \gamma}$, the inverse Gertsenshtein photons introduce a small distortion ΔF_γ to the CMB photon distribution which is otherwise assumed to be in equilibrium, i.e.,

$$\Delta F_\gamma(f, T) = F_\gamma(f, T) - F_{\text{eq}}(f, T), \quad (2.4)$$

where F_γ is the overall photon distribution, and F_{eq} describes the blackbody distribution of CMB photons

$$F_{\text{eq}} = \frac{1}{e^{f/f_{\text{eq}}} - 1}. \quad (2.5)$$

We analogously define a graviton distribution $F_g(f, T)$ to be

$$F_g = \frac{\pi^4}{15} \left(\frac{f_{\text{eq}}}{f} \right)^4 \left(\frac{\Omega_{\text{GW}}}{\Omega_\gamma} \right), \quad (2.6)$$

such that the total GW energy is obtained as

$$\rho_g = \int 16\pi^2 f^4 F_g(f, T) d \ln f = \rho_{\text{crit}} \int \Omega_{\text{GW}}(f) d \ln f, \quad (2.7)$$

where $\Omega_{\text{GW}}(f)$ is the GW energy density in units of the critical density.

The distribution functions $F_{\gamma, g}$ satisfy the Boltzmann equation,

$$\hat{L} F_{\gamma, g} = \pm (F_g - F_\gamma) \langle \Gamma_{\gamma g} \rangle, \quad (2.8)$$

where $\hat{L} = \partial_t - H f \partial_f = -H(T \partial_T + f \partial_f) \approx -HT \partial_T$ is the Liouville operator with H being the Hubble parameter, and $\partial_f F_{\gamma, g} = 0$ is assumed as we focus on conversions occurring at a fixed frequency. Here $\langle \Gamma_{\gamma g} \rangle$ is the conversion rate, such that it integrates to the total probability along the line-of-sight (l.o.s.) $\mathcal{P}_{g \rightarrow \gamma} = \int_{\text{l.o.s.}} \langle \Gamma_{\gamma g} \rangle dt$. The solution of (2.8) can be obtained as [52]

$$\begin{pmatrix} F_\gamma(f, T) \\ F_g(f, T) \end{pmatrix} = e^{-\mathcal{P}_{g \rightarrow \gamma}} \begin{pmatrix} \cosh \mathcal{P}_{g \rightarrow \gamma} & \sinh \mathcal{P}_{g \rightarrow \gamma} \\ \sinh \mathcal{P}_{g \rightarrow \gamma} & \cosh \mathcal{P}_{g \rightarrow \gamma} \end{pmatrix} \begin{pmatrix} F_\gamma(f T_{\text{ini}}/T, T_{\text{ini}}) \\ F_g(f T_{\text{ini}}/T, T_{\text{ini}}) \end{pmatrix}, \quad (2.9)$$

which, to the leading order in $\mathcal{O}(\mathcal{P}_{g \rightarrow \gamma})$, yields the expression for ΔF_γ as

$$\Delta F_\gamma(f_0, f_{\text{eq}}) = (F_g(f_{\text{ini}}, T_{\text{ini}}) - F_{\text{eq}}) \mathcal{P}_{g \rightarrow \gamma}. \quad (2.10)$$

Therefore, the fractional distortion to the photon distribution at a given frequency is

$$\frac{\Delta F_\gamma}{F_{\text{eq}}}(f) = \left[\frac{\pi^4}{15} \left(\frac{f_{\text{eq}}}{f} \right)^4 \left(\frac{\Omega_{\text{GW}}}{\Omega_\gamma} \right) (e^{f/f_{\text{eq}}} - 1) - 1 \right] \mathcal{P}_{g \rightarrow \gamma}, \quad (2.11)$$

where we assumed $F_\gamma = F_{\text{eq}}$ at the initial time. Inverting equation (2.11) yields a constraint on the GW energy density Ω_{GW} given by $\Delta F_\gamma/F_\gamma$ as

$$\Omega_{\text{GW}} = \frac{15}{\pi^4} \Omega_\gamma \left(\frac{\Delta F_\gamma}{F_{\text{eq}}} \mathcal{P}_{g \rightarrow \gamma}^{-1} + 1 \right) (e^{f/f_{\text{eq}}} - 1)^{-1} \left(\frac{f_{\text{eq}}}{f} \right)^{-4}. \quad (2.12)$$

Note that in similar works, sometimes the constraints are instead placed on the characteristic GW strain h_c , related to Ω_{GW} via

$$h_c(f) = \left(\frac{3H_0^2}{4\pi^2} \Omega_{\text{GW}}(f) f^{-2} \right)^{1/2}. \quad (2.13)$$

In further sections, we will analyse the measurements by directly associating the distortion of the blackbody temperature to that of the photon distribution in equation (2.11),

$$\frac{\Delta F_\gamma}{F_{\text{eq}}} = \frac{(e^{f/f_\gamma} - 1)^{-1} - (e^{f/f_{\text{eq}}} - 1)^{-1}}{(e^{f/f_{\text{eq}}} - 1)^{-1}} = \frac{e^{f/f_{\text{eq}}} - e^{f/f_\gamma}}{e^{f/f_\gamma} - 1}, \quad (2.14)$$

where $f_\gamma = k_B T_\gamma / (2\pi\hbar)$ is the characteristic frequency of a black body with temperature T_γ and an overall distribution F_γ . Explicitly in the Rayleigh-Jeans limit ($f \ll f_{\text{eq}} \approx 56.79$ GHz) and the high-frequency limit ($f \gg f_{\text{eq}} \approx 56.79$ GHz), equation (2.14) takes the forms

$$\frac{\Delta F_\gamma}{F_{\text{eq}}} \approx \begin{cases} \frac{f_\gamma - f_{\text{eq}}}{f_{\text{eq}}} = \frac{\Delta T}{T_{\text{CMB}}} & (f \ll f_{\text{eq}} \approx 56.79 \text{ GHz}), \\ e^{f \left(\frac{1}{f_{\text{eq}}} - \frac{1}{f_\gamma} \right)} - 1 = e^{\frac{f}{f_\gamma} \frac{\Delta T}{T_{\text{CMB}}}} - 1 & (f \gg f_{\text{eq}} \approx 56.79 \text{ GHz}), \end{cases} \quad (2.15)$$

where ΔT denotes the excess temperature on top of the CMB blackbody spectrum. Assuming that the inverse Gertsenshtein effect is the only mechanism causing such distortion, then $\delta T_g = \Delta T$, where δT_g is the temperature of graviton-induced photons. In reality, many mechanisms can potentially contribute and therefore $\delta T_g < \Delta T$ (see Section 3.1 for one such example and Sections 5.1 and 5.2 for discussions).

3 Existing measurements

We now present the constraints on the HFGWs from currently available measurements.

3.1 Kinematic Sunyaev-Zel'dovich effect

The kSZ effect has been conventionally used as a method to observe and study galaxy clusters since the induced CMB distortions act as markers for the underlying electron distribution in these clusters.

We provide a brief description of the kSZ modelling and refer the interested readers to Ref. [123] for more detail. The temperature contrast observed against the CMB can be characterised as [66]

$$\frac{\delta T_{\text{kSZ}}}{T_{\text{CMB}}} = \frac{\sigma_T}{c} \int_{\text{l.o.s.}} e^{-\tau} n_e v_p dl, \quad (3.1)$$

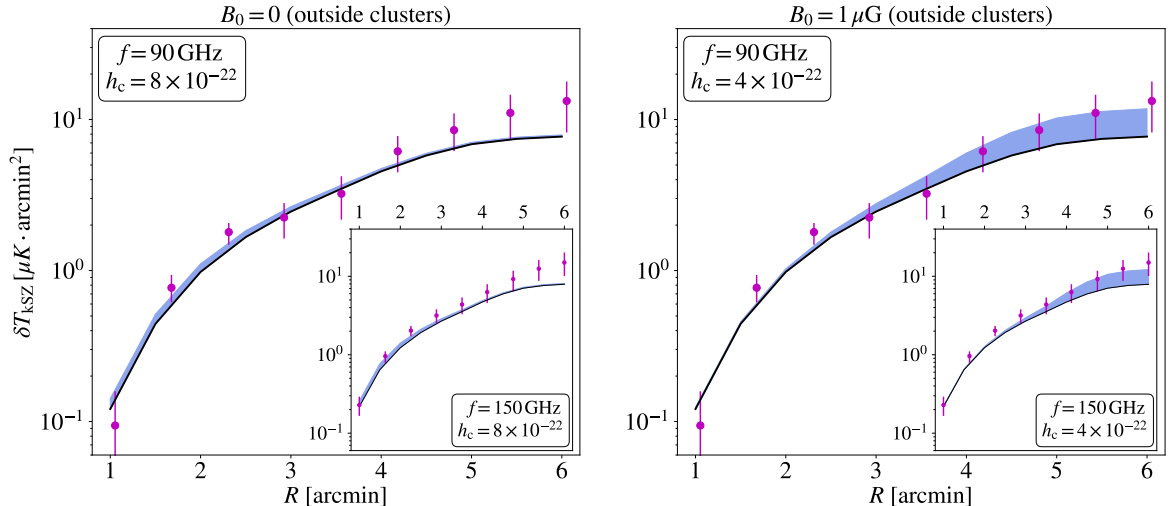


Figure 1: In both panels, ACT observations [65] are indicated by the purple dots and their error bars, and the kSZ temperature spectrum δT_{kSZ} from the baryon physics modelling [123] is shown in black solid lines. The effects of graviton-induced photons are indicated by blue shaded regions, assuming the absence of magnetic fields outside clusters and a background of HFGWs with strain $h_c = 8 \times 10^{-22}$ (left panel) and the presence of magnetic fields with strength $B_0 = 1 \mu\text{G}$ and HFGWs with $h_c = 4 \times 10^{-22}$ (right panel). The main panels and the insets respectively correspond to the cases of $f = 90 \text{ GHz}$ and $f = 150 \text{ GHz}$.

where σ_T is the Thomson cross-section, v_p is the peculiar velocity of the observed galaxies, and $\tau(\theta)$ is the optical depth along the line of sight (l.o.s.). The kSZ temperature in the above equation can be simplified in the observed redshift range of ACT, $0.4 < z < 0.7$ [65], by approximating $e^{-\tau} \approx 1$. In addition, the root-mean-square (rms) peculiar velocity along the l.o.s. is $v_p^{\text{rms}}/c \sim 1.06 \times 10^{-3}$. Therefore, equation (3.1) is determined essentially by the electron density n_e alone

$$\frac{\delta T_{\text{kSZ}}}{T_{\text{CMB}}} \approx 1.06 \times 10^{-3} \sigma_T \int_{\text{l.o.s.}} n_e dl, \quad (3.2)$$

where n_e , in turn, depends on the gas density ρ_{gas} . Modelling the baryonic physics that affects the gas distribution requires detailed hydrodynamical simulations [e.g. 124, 125]. However, we use an approximate method, called baryonic correction model (BCM), that are computationally less expensive and validated against advanced hydrodynamical simulations [126, 127]. We briefly describe this model in Appendix B. Reproducing the measurements provided by ACT requires convolving our model with the telescope filters, which are described in Ref. [65]. We refer the interested readers to Refs. [66, 123] for detailed modelling of this ACT observation.

Along with the kSZ effect, the temperature excess over the CMB can also receive a contribution from the inverse Gertsenshtein effect as HFGWs propagate through galactic and cluster magnetic fields. We assume that the total measured temperature contrast $\Delta T = \delta T_{\text{kSZ}} + \delta T_g$ with δT_g being the temperature of graviton-induced photons. The effect of varying the baryon distribution inside clusters by incorporating δT_g can be seen in Figure 1. The black line corresponds to a BCM with $\Delta T_g = 0$, aligning closely with the measurements within the 95% credible region sourced from Ref. [123]. The combined temperature profile ΔT is tuned to stay within the error margins of ACT datasets. We note that δT_g enhances

the overall temperature profile but the exact features depend on the magnetic field properties. Assuming that magnetic fields exist only inside the clusters and become absent in the ICM (left panel of Figure 1), the enhancement diminishes for the corresponding scales outside individual clusters. In this case, the strongest constraint, $h_c \geq 8 \times 10^{-22}$, takes place at the smallest angular scale $R \approx 1$, i.e., closest to the center of the cluster, corresponding to the largest GW propagation distance. Assuming uniform magnetic field $B_0 = 1 \mu\text{G}$ throughout the entire field of observation of $R \sim 6$ arcmin, corresponding to the scale ~ 3.7 Mpc at the mean redshift $z \sim 0.55$ (right panel of Figure 1), the temperature profile amplifies more with increasing angular scales. In this case, GW strains are upper bounded at the largest observed scales $R \approx 6$, giving $h_c \geq 4 \times 10^{-22}$. Therefore, detailed knowledge of magnetic fields within clusters and in the ICM is needed to determine precisely the effects of δT_g , although the results of the two assumptions shown in the left and right panels of Figure 1 differ within a factor of two. Using equations (2.12) and (2.15), and assuming the scenario of uniform magnetic fields throughout the field of observation, we note that the kSZ observations of ACT provide upper limits on the HFGW energy density $\Omega_{\text{GW}}(f)$ and strains $h_c(f)$, i.e., $\Omega_{\text{GW}} \lesssim 3.5 \times 10^{15}$ and $h_c \lesssim 8 \times 10^{-22}$ at $f = 90$ GHz, and $\Omega_{\text{GW}} \lesssim 9.9 \times 10^{15}$ and $h_c \lesssim 4 \times 10^{-22}$ at $f = 150$ GHz. We find that the inverse Gertsenshtein effect is a subdominant correction on top of the more significant kSZ effect, i.e., $\delta T_g \ll \delta T_{\text{kSZ}}$ for all observed angular scales, even for the unrealistically large HFGW amplitudes considered here.

3.2 Excess radio background

Previous studies have reported an excess of radio background through various methods, including direct measurements from ARCADE2 [128] and LWA1 [129], as well as indirect observations through the 21-cm signal during cosmic dawn. This 21-cm signal can be observed by radio experiments as the differential brightness temperature at position \mathbf{x} and redshift z , which is given as [67, 75]

$$\delta T_b(\mathbf{x}, z) = 27 \text{ mK} \left(\frac{0.15}{\Omega_m h^2} \frac{1+z}{10} \right)^{\frac{1}{2}} \left(\frac{\Omega_b h^2}{0.023} \right) x_{\text{HI}}(\mathbf{x}, z) [1 + \delta_b(\mathbf{x}, z)] \left[1 - \frac{T_{\text{radio}}(z)}{T_s(\mathbf{x}, z)} \right], \quad (3.3)$$

where x_{HI} , δ_b and T_s are neutral hydrogen fraction, baryon overdensity and spin temperature, respectively. This signal is observed against a radio background, which follows a blackbody spectrum of temperature T_{radio} .

The previously assumed radio background to be the CMB has been challenged by measurements from ARCADE2 [128] and LWA1 [129]. These measurements indicate the presence of excess radio signal over the CMB, denoted as $T_{\text{radio}} \neq T_{\text{CMB}}(1+z)$ [128, 129]. Additionally, the unconventional sky-averaged 21-cm signal evolution detected by EDGES [70] at $z \approx 17$ further supports the plausibility of this excess radio signal [69]. This radio background can be effectively described by the model:

$$T_{\text{radio}} = T_{\text{CMB}}(1+z) \left[1 + A_r \left(\frac{\nu_{\text{obs}}}{78 \text{ MHz}} \right)^\beta \right], \quad (3.4)$$

where A_r represents the frequency-independent amplitude coefficient, and $\beta \approx -2.55$ stands for the spectral index. Note that the bounds on $\Omega_{\text{GW}}(f)$ in equation (2.12) can be rewritten in terms of the A_r parameter as

$$\Omega_{\text{GW}}(f) = \frac{15}{\pi^4} \Omega_\gamma \left[A_r \left(\frac{\nu_{\text{obs}}}{78 \text{ MHz}} \right)^\beta \mathcal{P}_{g \rightarrow \gamma}^{-1} + 1 \right] \left(\frac{f_{\text{eq}}}{f} \right)^{-3}, \quad (3.5)$$

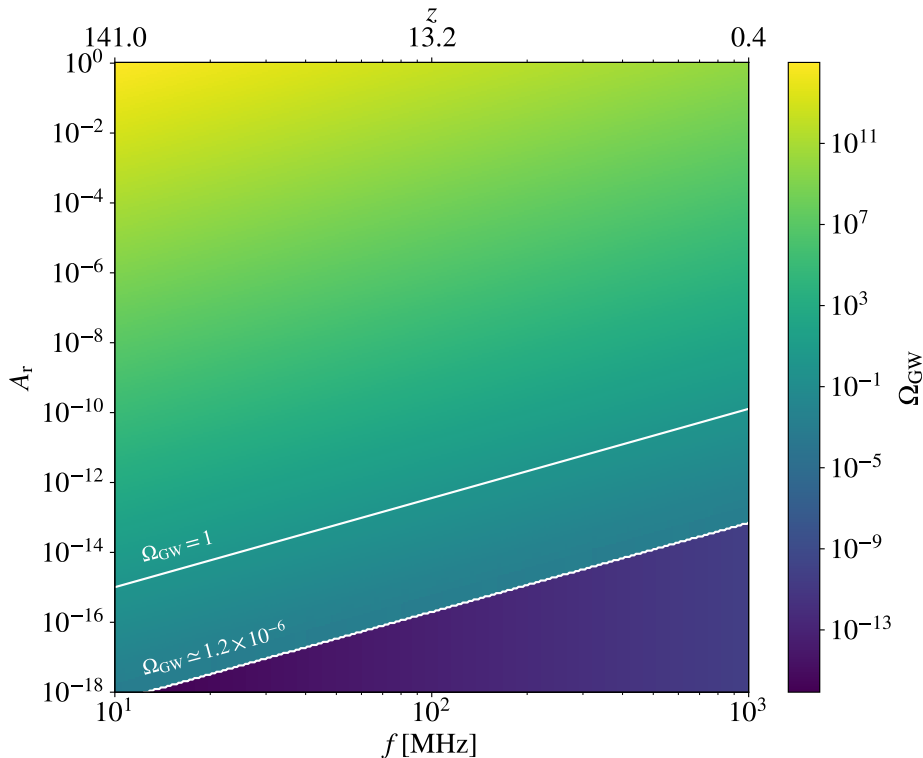


Figure 2: The upper limits of GW energy density $\Omega_{\text{GW}}(f)$ imposed by a range of corresponding values of the parameter A_r in equation (3.4), assuming cosmological magnetic fields with properties discussed in Section 2.2. The two white lines respectively indicate the A_r values necessary to reach the critical value of $\Omega_{\text{GW}} = 1$ and the ΔN_{eff} limit of $\Omega_{\text{GW}} \simeq 1.2 \times 10^{-6}$.

where the temperature distortion is given by $\Delta T/T_{\text{CMB}} = A_r(\nu_{\text{obs}}/78 \text{ MHz})^\beta$, and we have taken the Rayleigh-Jeans limit $f \ll f_{\text{eq}}$ applicable to the radio frequency regime.

Figure 2 demonstrates the upper bounds of $\Omega_{\text{GW}}(f)$ in equation (3.5), given certain values of A_r and a cosmological magnetic field with properties normalised in equation (2.2). To give an intuition of the constraining power of A_r , we compare to two theoretical expectations, namely the critical energy density $\Omega_{\text{GW}} = \Omega_{\text{crit}} = 1$, and the more realistic ΔN_{eff} bound given by

$$\Omega_{\text{GW}} \lesssim \frac{7}{8} \left(\frac{4}{11} \right)^{4/3} \Omega_\gamma \Delta N_{\text{eff}} \simeq 1.2 \times 10^{-6}, \quad (3.6)$$

where the variation of the effective number of relativistic degrees of freedom is measured to be $\Delta N_{\text{eff}} \lesssim 0.1$ [10, 130, 131], and the radiation energy density is $\Omega_\gamma \simeq 5.4 \times 10^{-5}$ [10]. For example, to constrain the $\Omega_{\text{GW}} \lesssim 1(1.2 \times 10^{-6})$ at $f \sim 100 \text{ MHz}$, we need to explore $A_r \lesssim 10^{-13}(10^{-16})$.

We can also use the measurements from radio telescopes such as LOFAR and MWA to constrain A_r . These telescopes are attempting to statistically measure the spatial distribution of δT_b with the 21-cm power spectrum during the epoch of reionisation [e.g. 73]. The field of view of these telescope are large enough for the signal to contain cosmological information, which has been used by previous authors to study cosmology [80, 134, 135]. To provide a conservative limit, we assume that the entire excess radio signals were created by

Instrument	z	f [MHz]	A_r	$\Delta T(z)$ [K]	$\Omega_{\text{GW}}(f)$	$h_c(f)$
EDGES	17.0	78	$\lesssim 1.9$	$\lesssim 90.49$	$\lesssim 9.69 \times 10^{12}$	$\lesssim 2.38 \times 10^{-20}$
LOFAR	9.1	141	$\lesssim 15.9$	$\lesssim 120.92$	$\lesssim 1.86 \times 10^{13}$	$\lesssim 1.85 \times 10^{-20}$
MWA	8.7	147	$\lesssim 79.4$	$\lesssim 439.71$	$\lesssim 8.37 \times 10^{13}$	$\lesssim 3.78 \times 10^{-20}$
	8.2	155	$\lesssim 75.9$	$\lesssim 351.58$	$\lesssim 6.98 \times 10^{13}$	$\lesssim 3.27 \times 10^{-20}$
	7.8	162	$\lesssim 74.1$	$\lesssim 296.02$	$\lesssim 6.09 \times 10^{13}$	$\lesssim 2.92 \times 10^{-20}$
	7.2	174	$\lesssim 25.1$	$\lesssim 92.08$	$\lesssim 1.72 \times 10^{13}$	$\lesssim 1.45 \times 10^{-20}$
	6.8	183	$\lesssim 10.0$	$\lesssim 42.69$	$\lesssim 6.04 \times 10^{12}$	$\lesssim 8.16 \times 10^{-21}$
	6.5	190	$\lesssim 2.5$	$\lesssim 22.99$	$\lesssim 1.37 \times 10^{12}$	$\lesssim 3.74 \times 10^{-21}$

Table 1: Bounds of GW energy density $\Omega_{\text{GW}}(f)$, characteristic strain $h_c(f)$, and the corresponding radio temperature excess $\Delta T(z)$ from existing observations of EDGES [69], LOFAR [132], and MWA [133] in the $\mathcal{O}(10^2)$ MHz regime. We also show the corresponding redshift z along with the A_r values constrained at 68% confidence level.

inverse Gertsenshtein effect. We then use equations (3.4) and (2.15) to convert the values of $A_r \neq 0$ reported by authors interpreting observations from EDGES [69], LOFAR [132], and MWA [133] to constraints on the GW energy density $\Omega_{\text{GW}}(f)$ and characteristic strain $h_c(f)$ at the corresponding frequency f^3 . Note that this is done assuming magnetic field properties normalised in equation (2.2). The resulting constraints on GWs at MHz frequencies are shown in Table 1. Though several orders of magnitude weaker than the ΔN_{eff} bound, these constraints have been derived from independent measurements. Previous studies have explored several phenomena, including emission from high redshift radio galaxies [72] and superconducting cosmic strings [137], to explain the excess radio background. If such phenomena are confirmed to contribute to this excess signal, then the constraints on GWs can be improved further.

In Table 2, we have listed measurements from ARCADE2 [138] that directly measure the photon background at GHz frequencies, encompassing both the CMB and GWs converted into photons. ΔT_0 gives the measured excess temperature over the CMB at different frequencies (f). This table also includes constraints on GHz frequency GWs via equation (2.15), albeit being relatively weak. We anticipate improvements in these constraints with upcoming CMB experiments, which will be elaborated upon in Section 4.2.

4 Future surveys

We will now discuss the future surveys that are capable of improving the constraints on HFGWs. First, we present a forecast study for the upcoming radio telescope, the Square Kilometre Array (SKA). Later, we will discuss the potential of future CMB experiments.

4.1 Forecast with the SKA

The observation of the 21-cm signal will improve substantially with the SKA that is currently under construction at two different sites. Here we will focus on the low-frequency component built in Western Australia that will cover frequencies $f \sim 30 - 300$ MHz [75]. In this study, we

³For the Hydrogen Epoch of Reionization Array (HERA), Ref. [136] have studied models with excess radio background. However, the constraints are provided on T_s/T_{radio} , which is not straightforward to convert to our parameterisation based on A_r . Therefore we excluded this dataset from this work.

Instrument	f [GHz]	ΔT_0 [K]	$\Omega_{\text{GW}}(f)$	$h_c(f)$
ARCADE2	3.2	$\lesssim 0.0615$	$\lesssim 2.60 \times 10^{11}$	$\lesssim 9.63 \times 10^{-23}$
	3.4	$\lesssim 0.0445$	$\lesssim 2.00 \times 10^{11}$	$\lesssim 7.93 \times 10^{-23}$
	7.9	$\lesssim 0.0355$	$\lesssim 3.58 \times 10^{11}$	$\lesssim 4.53 \times 10^{-23}$
	8.3	$\lesssim 0.0175$	$\lesssim 1.84 \times 10^{11}$	$\lesssim 3.11 \times 10^{-23}$
	9.7	$\lesssim 0.0055$	$\lesssim 6.65 \times 10^{10}$	$\lesssim 1.60 \times 10^{-23}$
	10.5	$\lesssim 0.0125$	$\lesssim 1.62 \times 10^{11}$	$\lesssim 2.32 \times 10^{-23}$

Table 2: Bounds of GW energy density $\Omega_{\text{GW}}(f)$, characteristic strain $h_c(f)$, and the corresponding radio temperature excess ΔT_0 from ARCADE2 [138] in the $\mathcal{O}(10^0)$ GHz regime. Note that measurements of ARCADE2 at $f \in \{29.5, 31, 90\}$ GHz are not shown here as they are consistent with CMB.

will use the power spectra expected from the SKA that will quantify the spatial fluctuation strength of the 21-cm signal at different redshifts.

In order to model the power spectra, we use the analytical framework initially proposed in Ref. [139]. This framework has been actively improved to study the impact of cosmological structure formation on the 21-cm signal at high redshift ($z \gtrsim 6$) [79, 80]. We construct the mock observation for SKA using the open source package, `Tools21cm` [140]. The error in the measurement accounts for the instrumental noise that increases with increasing wavenumber (k). This noise was estimated assuming an observation time of 1000 hours and the latest plan of SKA antenna distribution. For a detailed description of this calculation, we refer the readers to Ref. [141]. We only consider the power spectra at $k \gtrsim 0.1 \text{ Mpc}^{-1}$ preventing the regime dominated by cosmic variance and foreground contamination [142].

We examine the identical mock observation illustrated in Figure 5, and the model parameters assumed during the observation listed under ‘Mock Value’ in Table I of Ref. [80]. These observations are constructed at 12 redshifts covering frequency $f \sim 80 - 200$ MHz. For this mock observation, the value of A_r is zero, which corresponds to no excess radio background. To infer the constraints expected on A_r , we performed an Monte Carlo Markov Chain (MCMC) analysis. We provide the full result in appendix C. This analysis constrained $A_r \lesssim 10^{-9}$ at 68% confidence level. With magnet field properties in equation (2.2), i.e., $B_0 \sim 0.1 \text{ nG}$ and $\Delta l_0 \sim 1 \text{ Mpc}$, this A_r value corresponds to $\Omega_{\text{GW}} \gtrsim 6.0 \times 10^4$ at $f \sim 30 \text{ MHz}$ and $\Omega_{\text{GW}} \gtrsim 4.7 \times 10^2$ at $f \sim 200 \text{ MHz}$. We show this constraint in Figure 3. Compared to the current limits at these MHz frequencies (Table 1), SKA will improve it by 7 to 10 orders of magnitude.

The reionisation and heating of the IGM by the first photon source or galaxies impact the spatial distribution of the signal at ionised bubble scales, which would have a scale dependent effect on the 21-cm signal [143–145]. This scale-dependent information in the SKA data will help constrain the early galaxy properties and allow constraining A_r with the amplitude of the spectrum [132]. However, we assume that the 21-cm background is uniformly amplified by primordial HFGWs. Therefore, the improvement we predict for the SKA is not sensitive to the assumed properties of the first galaxies for our mock observation. We also want to mention a caveat of our forecast study, which is the assumption that the foreground signal is assumed to be perfectly removed.

In this study, we assumed the sensitivity of the first phase of SKA. The later stages are planned to be more sensitive that will allow the constraints on HFGWs to be even stronger. We should also note that the constraints could also be improved with longer observation time.

Instrument	Status	f [GHz]	ΔT [nK]	f_{\min} [GHz]	$\Omega_{\text{GW}}(f_{\min})$	$h_c(f_{\min})$
PRISTINE	Proposed	[50, 1000]	181	1000	1.7×10^1	2.5×10^{-30}
PIXIE	Proposed	[10, 1000]	13	1000	1.2×10^2	6.7×10^{-30}
Super-PIXIE	Concept	[10, 1000]	10	1000	9.5×10^1	5.9×10^{-30}
Voyage 2050	Concept	[5, 3000]	3	3000	3.9×10^{-13}	1.3×10^{-37}

Table 3: Foreground- marginalised forecast detection capabilities of proposed CMB surveys PRISTINE, PIXIE/Super-PIXIE, and Voyage 2050. The tightest HFGW bounds $\Omega_{\text{GW}}(f_{\min})$ and the corresponding frequency f_{\min} are also shown. The magnetic field properties are chosen to be in line with equation (2.2).

However, processing large radio data is challenging due to various complexities, including the intricate process of data calibration (see Refs. [146, 147] and references therein). Therefore we have considered 1000 hour observation time, which is the initial target [75]. The SKA will be sensitive enough to give us measurements beyond the power spectrum, including the bispectrum [e.g. 148, 149] and image datasets [e.g. 143, 150, 151]. These measurements will have more constraining power, which we will explore in the future.

4.2 Forecast with future CMB surveys

In the future, a number of precision surveys of CMB and its spectral distortions could improve the constraints on HFGWs beyond the GHz regime. Here we consider the expected capabilities of proposed missions such as Polarized Radiation Interferometer for Spectral disTortions and INflation Exploration (PRISTINE) [152], the Primordial Inflation Explorer (PIXIE) [153, 154] and its next-generation concept Super-PIXIE, as well as the scheme Voyage 2050 [155], assumed to be a few times more sensitive than Super-PIXIE. We take the foreground-marginalized error budget for temperature measurements of these missions [152] and compute the upper limits of HFGW energy density $\Omega_{\text{GW}}(f)$ within the corresponding detectors' frequency bands. The anticipated temperature signal errors are shown in Table 3 for PRISTINE (2 years), PIXIE (4 years), Super-PIXIE (8 years), and Voyage 2050 [152]. Spectral distortions at $\mathcal{O}(10^{0-2})$ nK precision, if achieved, would significantly tighten the HFGW constraints, even reaching below the critical value $\Omega_{\text{GW}} = 1$ and the current ΔN_{eff} bound $\Omega_{\text{GW}} \simeq 1.2 \times 10^{-6}$ at the THz frequency regime. On the other hand, the ΔN_{eff} bound could also be tightened with these precision future surveys and a careful comparison between the expectations is needed. The forecast constraints from SKA and future CMB surveys are shown in Figure 3 together with the estimates from Sections 3.1 and 3.2. We show that PIXIE/super-PIXIE and, consequently, PRISTINE have the capability to significantly tighten constraints, bringing them into an intriguing range. Voyage 2050, which is at the conceptualisation phase, will substantially improve the constraints on HFGW probing $\Omega_{\text{GW}} \lesssim 1.2 \times 10^{-6}$ in the THz regime.

5 Discussions

In Section 5.1, we compare the sensitivity of ongoing and planned experiments to constrain HFGWs. Later in Section 5.2, we will briefly discuss a few more alternate methods.

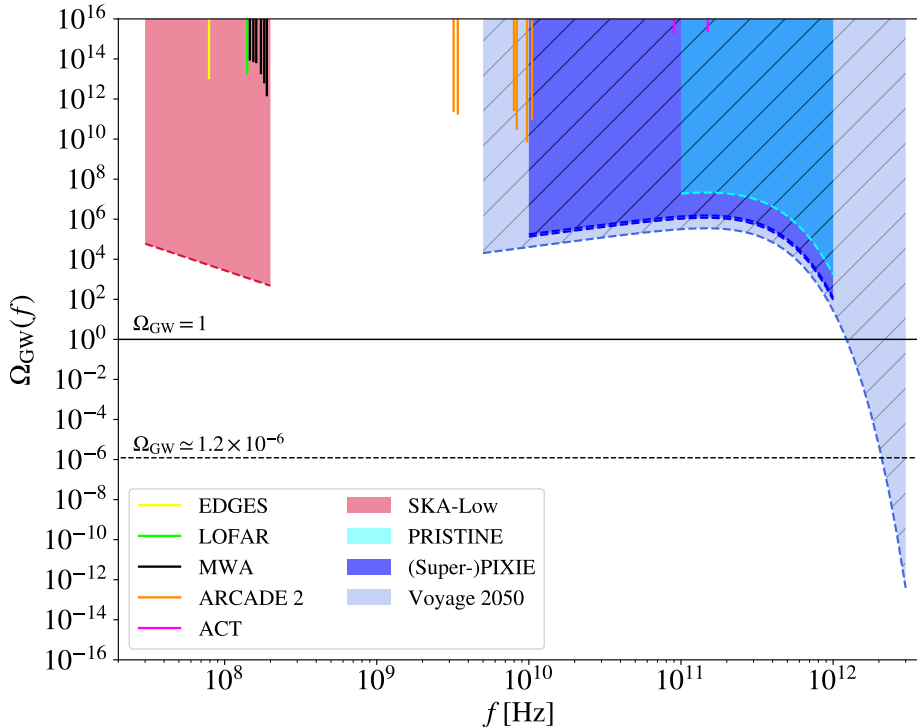


Figure 3: Upper limits of HFGW energy density $\Omega_{\text{GW}}(f)$ from existing measurements using EDGES (yellow) [69, 70], LOFAR (green) [132], MWA (black) [133], ARCADE2 (orange) [138], and ACT (purple) [65]. Forecast with the upcoming SKA-Low (red) is shaded in red. Forecast with proposed and conceptual PRISTINE (cyan) [152], PIXIE/Super-PIXIE (blue) [153, 154] and Voyage 2050 (light blue) [155] are also shown in comparison with tilted hatches. The black lines in the lower part of the figure indicate the theoretical upper bounds of GWs: the solid line shows where $\Omega_{\text{GW}} = 1$, and the dash-dotted line indicates the ΔN_{eff} bound from equation (3.6).

5.1 Sensitivity comparison

From Figure 3, we make the following observations regarding the constraints on HFGWs from existing and projected future detectors.

- Among the existing instruments, ARCADE2 provides the tightest constraint at $\Omega_{\text{GW}} \lesssim 10^{11}$, followed by radio telescopes EDGES, LOFAR, and MWA with similar constraints at $\Omega_{\text{GW}} \lesssim 10^{13}$. The least competitive constraints come from ACT at $\Omega_{\text{GW}} \lesssim 10^{16}$.
- The constraints from ACT are the least competitive due to the low conversion probability applicable to kSZ observations of individual galaxy clusters, i.e., $\mathcal{P} \sim 10^{-30}$ in equation (2.1). This is much lower than the conversion probability applicable for global radio excess signals, i.e., $\mathcal{P} \sim 10^{-20}$ in equation (2.2).
- Constraints obtained in this work using existing measurements are comparable to similar work in the literature [44, 52, 156], although a much tighter bound of $\Omega_{\text{GW}} < 1$ has been claimed in the X-ray frequency band [156].

- We found that all upcoming and future observations are significant improvements at their corresponding frequencies. Even with an realistic amount of observing time, i.e. 1000 hours, and the conservative assumption that graviton-induced photons saturate the entire excess signals, the SKA is expected to improve the existing constraints in the MHz frequency band by roughly 10 orders of magnitude to $\Omega_{\text{GW}} \lesssim 10^{2-4}$.
- Removing foreground contributions, proposed (PRISTINE, (Super-)PIXIE, Voyage 2050) CMB surveys can significantly tighten the Ω_{GW} upper limits, with Voyage 2050 reaching below the BBN bound in the THz regime, if the anticipated precisions are achieved. However, note that the results are highly dependent on the foreground modelling and that, as of the time of writing, these surveys remain a concept.
- Similar to the projected CMB surveys, our conservative estimates in the MHz to GHz regimes can be further improved by combining foreground contribution from other mechanisms, such as decays of relic neutrinos [157, 158], axions [159] and other dark matter candidates [160, 161]. We leave this to future studies.

5.2 Alternative methods to probe HFGW

Though this work focused on approach *(i)* introduced in Section 1, we want to discuss the ongoing efforts to explore approach *(ii)*. Many laboratory proposals exploit the similarities between axion-photon and graviton-photon couplings to constrain HFGWs using axion detectors. The QCD axions are pseudoscalars initially proposed as a dynamical solution to the strong charge-parity (CP) problem [162–165] (see Ref. [166] for a review of axions and axion-like particles). Numerous experimental efforts are underway to survey the parameter space of axions, due to their desirable properties as a dark matter candidate [167–169] (see Refs. [170–172] for reviews). The coupling between axion and EM fields reads $\mathcal{L} \supset g_{a\gamma} a F \tilde{F}$, where a is the axion field and $g_{a\gamma}$ the coupling strength. This resembles the coupling between gravity and the EM sector via the term $\mathcal{L} \supset h F^2$. The similarity implies that both axions and gravitons can convert to photons in external magnetic fields and that data from existing axion haloscopes can be reinterpreted to constrain HFGWs [58, 59]. In general, approach *(ii)* has the advantage of having full knowledge and control of the magnetic field. The properties of large-scale magnetic fields, on the other hand, have not been precisely constrained. However, the future SKA surveys have the potential to substantially improve our understanding about their origin and structure on large-scales [173]. Laboratory field strength (up to ~ 10 T) can also be much larger than cosmological fields as well, although the latter compensate by having a much larger effective detector volume. Besides the two approaches of the inverse Gertsenshtein effect overall, other methods to detect HFGWs have been proposed, based on the couplings between gravitons and materials or mediums other than EM waves. These include, but not limited to, quantum sensors to detect graviton-phonon conversion [174, 175], optically levitated sensors [176, 177], microwave cavities [178–181], bulk acoustic wave devices [182], and graviton-magnon resonance detectors [183]. Note that it is nontrivial to unify the sensitivity treatment and comparison across different detection proposals. Therefore, we leave the quantitative comparison of the advantages and disadvantages of the proposed methods to a future work.

6 Conclusion

In this work we estimated the upper bounds on the stochastic background of HFGWs at 16 frequency bands in the $\mathcal{O}(10^2)$ MHz and $\mathcal{O}(10^2)$ GHz regimes by applying the inverse Gertsenshtein effect to large-scale magnetic fields. The bounds are obtained conservatively by saturating with induced Gertsenshtein photons: (i) the excess of radio background over CMB reported by EDGES, LOFAR, MWA, and ARCADE2, and (ii) the error margins of the kSZ observations made by ACT, assuming a fixed underlying model of baryonic physics inside galaxy clusters. We note that these constraints are comparable in competitiveness as similar works, and that they all lie many orders of magnitude larger than the ΔN_{eff} bound. Therefore, probing a high-frequency SGWB using inverse Gertsenshtein effect might be challenging with the existing instruments.

However, the ΔN_{eff} bound as a benchmark only applies to SGWB produced before BBN at $T \sim 1$ MeV, and late-Universe mechanisms might generate GWs that reach above the bound $\Omega_{\text{GW}} \simeq 1.2 \times 10^{-6}$ at certain frequencies. In addition, for transient HFGW events, the theoretical bounds on a stochastic background also become invalid. Thus, albeit the challenges, inverse Gertsenshtein effect is worth careful further studies in different contexts as a means to probe HFGWs. It is especially so since significant improvements can be expected with future measurements. The upcoming SKA is expected to be much more sensitive than the current radio telescopes considered in this and other similar works. We forecast an approximately 10 orders of magnitude tighter constraint from SKA when applied in the context of excess radio background. Here we have only focused on the low frequency component of SKA that will observe the IGM during cosmic reionisation. The medium frequency component of SKA will observe the 21-cm signal produced by the neutral hydrogen inside galaxies [184] and help fill the gap seen in Figure 3 above $f \sim 200$ MHz. We will explore this regime in the future. Finally, the future CMB surveys anticipated to detect spectral distortions at $\mathcal{O}(10^{0-2})$ nK level could potentially reach the current ΔN_{eff} bound. Finally, obtaining more realistic upper limits of HFGWs requires careful considerations of realistic magnetic fields, possibly using direct numerical simulations, as well as going beyond the conservative estimations by saturating Gertsenshtein photons. This implies a detailed understanding of other systematic and/or physical mechanisms contributing to the global foreground signals.

Acknowledgments

We thank Sreenath K. Manikandan, Florian Niedermann, and Nikhil Sarin for useful discussions. We also thank Axel Brandenburg for a careful reading of the manuscript. Y.H. is partially supported through the grant No. 2019-04234 from the Swedish Research Council (Vetenskapsrådet). S.M. acknowledges financial support from the Cariplo “BREAKTHRU” fund (Rif: 2022-2088 CUP J33C22004310003). Nordita is sponsored by Nordforsk.

A Inverse Gertsenshtein formalism

In this appendix, we present some context for the inverse Gertsenshtein effect, including a derivation of the probability equation (2.1). See Refs. [31, 33, 52, 185] for similar formulations.

Equations of motion

To study the interaction between GW and EM waves, we consider a system consisting of gravity and EM fields minimally coupled to gravity

$$S = S_{\text{GR}} + S_{\text{EM}}^{(0)} + S_{\text{EM}}^{(1)}, \quad (\text{A.1})$$

where S_{GR} is the Einstein-Hilbert action, and $S_{\text{EM}}^{(0)}$ and $S_{\text{EM}}^{(1)}$ are respectively the Maxwell and Heisenberg-Euler [186] actions

$$S_{\text{GR}} = \frac{1}{2\kappa} \int d^4x \sqrt{-g} R, \quad (\text{A.2})$$

$$S_{\text{EM}}^{(0)} = - \int d^4x \sqrt{-g} \left(\frac{1}{4} F_{\mu\nu} F^{\mu\nu} - A_\mu J^\mu \right), \quad (\text{A.3})$$

$$S_{\text{EM}}^{(1)} = \frac{\alpha^2}{90m_e^4} \int d^4x \sqrt{-g} \left((F_{\mu\nu} F^{\mu\nu})^2 + \frac{7}{4} (\tilde{F}_{\mu\nu} F^{\mu\nu})^2 \right). \quad (\text{A.4})$$

Here $F_{\mu\nu} = \partial_\mu A_\nu - \partial_\nu A_\mu$ is the Faraday tensor, and $\tilde{F}^{\mu\nu} \equiv \epsilon^{\mu\nu\alpha\beta} F_{\alpha\beta}/2$ is its dual defined using the totally antisymmetric Levi-Civita symbol $\epsilon^{\mu\nu\alpha\beta}$, $\alpha = e^2/(4\pi)$ is the fine structure constant, and m_e is the electron mass. The Heisenberg-Euler action accounts for effective QED corrections in the low-frequency limit, $\omega \ll m_e \sim 10^{20}$ Hz [186, 187].

In terms of a metric perturbation such that $g_{\mu\nu} = \bar{g}_{\mu\nu} + h_{\mu\nu}$, where $\bar{g}_{\mu\nu}$ is the background and $h_{\mu\nu}$ is a small perturbation, we obtain the coupled Einstein-Maxwell equations of motion (EOMs) that are linear in $h_{\mu\nu}$

$$\square h_{\mu\nu} = -2\kappa T_{\mu\nu}, \quad (\text{A.5})$$

$$\partial_\mu \left[F^{\mu\nu} - \frac{\alpha^2}{45m_e^4} (4F^2 F^{\mu\nu} + 7(F \cdot \tilde{F}) \tilde{F}^{\mu\nu}) \right] + J^\nu = \partial_\mu (h^{\mu\beta} \bar{g}^{\nu\alpha} F_{\beta\alpha} - h^{\nu\beta} \bar{g}^{\mu\alpha} F_{\beta\alpha}), \quad (\text{A.6})$$

where $T_{\mu\nu}$ is the EM energy-momentum tensor

$$T_{\mu\nu} = \bar{g}^{\rho\sigma} F_{\mu\rho} F_{\nu\sigma} - \frac{1}{4} \bar{g}_{\mu\nu} F^2. \quad (\text{A.7})$$

From the modified Maxwell equation (A.6), note that the QED corrections can be neglected if they are subdominant compared to the current. The limit where this occurs can be obtained as follows. We identify the EM current as

$$J^\nu = -\omega_{\text{pl}}^2 A^\nu, \quad (\text{A.8})$$

where $\omega_{\text{pl}}^2 = e^2 n_e / m_e$ is the plasma frequency, with n_e being the electron number density. In galaxies and clusters, the density is typically $n_e \sim 10^{-3} \text{ cm}^{-3}$, giving a plasma frequency of $\omega_{\text{pl}} \sim \mathcal{O}(10^3)$ Hz.

The relevance of the nonlinear QED terms in (A.6) can be estimated by noting

$$F^2 = 2(\mathbf{B}^2 - \mathbf{E}^2) = \mathcal{O}(\mathbf{B}^2), \quad F\tilde{F} = 4\mathbf{B} \cdot \mathbf{E} \ll \mathcal{O}(\mathbf{B}^2), \quad (\text{A.9})$$

where we have assumed $|E| \ll |B|$. In comparison to the EM current (A.8), the QED corrections become important if the magnetic field satisfies

$$\left(\frac{B}{B_{\text{crit}}} \right) \left(\frac{\omega}{\omega_{\text{pl}}} \right) \gtrsim \frac{3}{2\alpha} \sqrt{\frac{5}{2}}, \quad (\text{A.10})$$

where $B_{\text{crit}} = m_e^2 \sim 10^{13} \text{ G}$ is a critical value. In the relevant regimes we consider, i.e., $B \sim \mu\text{G}$ and $\omega \lesssim \mathcal{O}(10^2) \text{ GHz}$, the condition (A.10) is clearly not satisfied. Therefore, we neglect the QED corrections and reduce the Maxwell equation (A.6) to

$$(\square - \omega_{\text{pl}}^2)A^\nu = -\bar{g}^{\mu\alpha}\bar{F}_{\beta\alpha}\partial_\mu h^{\nu\beta}, \quad (\text{A.11})$$

where we have split the Faraday tensor $F_{\mu\nu} = \bar{F}_{\mu\nu} + f_{\mu\nu}$ into a quasi-static background $\bar{F}_{\mu\nu}$ and a small perturbation $|f_{\mu\nu}| \ll \bar{F}_{\mu\nu}$ induced by GWs. We also used the Lorenz gauge for both EM and GW quantities, i.e., $\partial_\mu A^\mu = \partial_\mu h^{\mu\nu} = 0$.

Conversion probability

The GW equation (A.5) in terms of its components reads

$$\square \begin{pmatrix} h_{11} & h_{12} \\ h_{21} & h_{22} \end{pmatrix} = -2\kappa \begin{pmatrix} \frac{1}{2}(-B_1^2 + B_2^2 + B_3^2) & B_1 B_2 \\ B_1 B_2 & \frac{1}{2}(B_1^2 - B_2^2 + B_3^2) \end{pmatrix}, \quad (\text{A.12})$$

where the EM tensor (A.7) is assumed to be dominated by the magnetic fields

$$T_{ij} = E_i E_j + B_i B_j - \frac{1}{2}(\mathbf{E}^2 + \mathbf{B}^2)\delta_{ij} \approx B_i B_j - \frac{1}{2}\mathbf{B}^2\delta_{ij}. \quad (\text{A.13})$$

As a result of the split of the Faraday tensor, the magnetic field ($B = \bar{B} + b$) also decomposes into a homogeneous part \bar{B} and a small induced part $|b| \ll |\bar{B}|$. To bilinear order in \bar{B} and b , and let $\partial_i = (0, 0, \partial_l)$ in the longitudinal direction only, then the induced magnetic fields are $(b_1, b_2, b_3) = (-\partial_l A_2, \partial_l A_1, 0)$ and equation (A.12) becomes

$$\square \begin{pmatrix} h_{11} & h_{12} \\ h_{21} & h_{22} \end{pmatrix} = -2\kappa \begin{pmatrix} (\bar{B}_1 \partial_l A_2 + \bar{B}_2 \partial_l A_1) & (\bar{B}_1 \partial_l A_1 - \bar{B}_2 \partial_l A_2) \\ (\bar{B}_1 \partial_l A_1 - \bar{B}_2 \partial_l A_2) & -(\bar{B}_1 \partial_l A_2 + \bar{B}_2 \partial_l A_1) \end{pmatrix}. \quad (\text{A.14})$$

Without loss of generality, we rotate $(B_1, B_2) \rightarrow (B, 0)$ in the transverse plane, and denote $\lambda = \{+, \times\}$ such that $h_{11} = -h_{22} = h_+$, $h_{12} = h_{21} = h_\times$ and $A_1 = A_\times$, $A_2 = A_+$. Then the GW equation (A.14) simplifies to

$$\square h_\lambda = -2\kappa \bar{B} \partial_l A_\lambda. \quad (\text{A.15})$$

Similarly the Maxwell equation (A.11) can be recast to

$$(\square - \omega_{\text{pl}}^2) \begin{pmatrix} A^{(1)} \\ A^{(2)} \end{pmatrix} = \begin{pmatrix} \partial_l h^{(11)} & \partial_l h^{(12)} \\ \partial_l h^{(21)} & \partial_l h^{(22)} \end{pmatrix} \begin{pmatrix} \bar{B}_2 \\ -\bar{B}_1 \end{pmatrix}, \quad (\text{A.16})$$

which, in the same frame of $(B_1, B_2) \rightarrow (B, 0)$ as above, leads to the simplified form of

$$(\square - \omega_{\text{pl}}^2)A_\lambda = -\bar{B}\partial_l h_\lambda. \quad (\text{A.17})$$

We approximate $\square = \omega^2 + \partial_l^2 = (\omega + i\partial_l)(\omega - i\partial_l) \simeq 2\omega(\omega + i\partial_l)$, where we assumed $\partial_0 \simeq -i\omega$, $-i\partial_l \simeq k$ and $\omega + k \simeq 2\omega$. Note that we expressed the wavenumber k in terms of ω using dispersion relation $k = \mu\omega$, and used the fact that $\mu - 1 \ll 1$ in our case to arrive at $\omega + k \simeq 2\omega$. We also focus on monochromatic waves such that $A_\lambda(t, l) = e^{-i\omega t} A_\lambda(l)$ and $h_\lambda(t, l) = e^{-i\omega t} h_\lambda(l)$. Then the spatial solution $A_\lambda(l)$ and $h_\lambda(l)$ in the system of equations (A.17) and (A.15) can be written as

$$[\omega + i\partial_l - \omega(1 - \mu)]A_\lambda(l) + \frac{i}{2}\bar{B}h_\lambda(l) = 0, \quad (\omega + i\partial_l)h_\lambda(l) + i\kappa\bar{B}A_\lambda(l) = 0, \quad (\text{A.18})$$

where μ is the refractive index

$$\mu = \sqrt{1 - (\omega_{\text{pl}}/\omega)^2}. \quad (\text{A.19})$$

equations (A.18) can be further summarised as

$$(\omega + i\partial_l + \mathcal{M})\psi(l) = 0, \quad (\text{A.20})$$

where $\psi(l) = (A_\lambda(l), h'_\lambda(l))^T$ denotes the desired solution with $h'_\lambda(l) = h_\lambda(l)/\sqrt{2\kappa}$ (we drop the prime from here on), and the matrix \mathcal{M} reads

$$\mathcal{M} = \begin{pmatrix} \Delta_{\gamma\gamma} & -i\Delta_{\gamma g} \\ -i\Delta_{\gamma g} & 0 \end{pmatrix} = \begin{pmatrix} -\omega(1 - \mu) & -i\bar{B}\sqrt{\kappa/2} \\ -i\bar{B}\sqrt{\kappa/2} & 0 \end{pmatrix}. \quad (\text{A.21})$$

The relevant eigenvalues $m_{1,2}$ and the corresponding diagonal matrix are

$$m_{1,2} = \frac{1}{2} \left[\Delta_{\gamma\gamma} \pm \sqrt{\Delta_{\gamma\gamma}^2 - 4\Delta_{\gamma g}^2} \right], \quad \mathcal{D} = \begin{pmatrix} m_1 & 0 \\ 0 & m_2 \end{pmatrix}. \quad (\text{A.22})$$

We then rotate the solution to $\psi \rightarrow \psi' = \mathcal{U}\psi$ with a unitary matrix \mathcal{U} ,

$$\mathcal{U} = \begin{pmatrix} \cos\theta & \sin\theta \\ -\sin\theta & \cos\theta \end{pmatrix}, \quad \tan 2\theta = \frac{2\Delta_{\gamma g}}{\Delta_{\gamma\gamma}}, \quad (\text{A.23})$$

such that $\mathcal{U}^{-1} = \mathcal{U}^T$ and $\mathcal{U}\mathcal{M}\mathcal{U}^{-1} = \mathcal{D}$. Then in the rotated plane, (A.20) becomes

$$(\omega + i\partial_l + \mathcal{D})\psi'(l) = 0, \quad (\text{A.24})$$

with its solution

$$\psi'(l) = e^{i(\omega + \mathcal{D})l} \psi'_{\text{ini}}(l_{\text{ini}}). \quad (\text{A.25})$$

Rotating back to the original solution space yields

$$\psi(l) = e^{i\omega l} (\mathcal{U}^T e^{i\mathcal{D}l} \mathcal{U}) \psi_{\text{ini}}(l_{\text{ini}}) = e^{i\omega l} \mathcal{K} \psi_{\text{ini}}(l_{\text{ini}}), \quad (\text{A.26})$$

where $\psi_{\text{ini}}(l_{\text{ini}}) = (A_{\lambda,\text{ini}}, h_{\lambda,\text{ini}})^T$ denotes the initial conditions and the matrix \mathcal{K} gives the amplitude coefficients

$$\mathcal{K} = \begin{pmatrix} \mathcal{K}_{11} & \mathcal{K}_{12} \\ \mathcal{K}_{21} & \mathcal{K}_{22} \end{pmatrix} = \begin{pmatrix} [\cos^2\theta e^{im_1 l} + \sin^2\theta e^{im_2 l}] & [\cos\theta \sin\theta (e^{im_1 l} - e^{im_2 l})] \\ [\cos\theta \sin\theta (e^{im_1 l} - e^{im_2 l})] & [\sin^2\theta e^{im_1 l} + \cos^2\theta e^{im_2 l}] \end{pmatrix}. \quad (\text{A.27})$$

By starting with an initial state with only GWs and no EM waves, i.e., $\psi_{\lambda,\text{ini}} = (0, 1)^T$, we note that the sum of the squared coefficients in front of $h_{\lambda,\text{ini}}$ is conserved, i.e., $|\mathcal{K}_{12}|^2 + |\mathcal{K}_{22}|^2 = 1$. Therefore, the graviton-photon conversion probability can be interpreted as the off-diagonal amplitude $|\mathcal{K}_{12}|^2$, i.e.,

$$P(l) = |\langle h_{\lambda,\text{ini}} | A_\lambda(l) \rangle|^2 = |\cos\theta \sin\theta (e^{im_1 l} - e^{im_2 l})|^2 = \frac{1}{2} \kappa (\bar{B} l_{\text{osc}})^2 \sin^2(l/l_{\text{osc}}), \quad (\text{A.28})$$

where we used $\sin(\tan^{-1} \zeta) = \zeta/\sqrt{1 + \zeta^2}$, and identified an oscillation length scale l_{osc} from the two eigenvalues $m_{1,2}$ in (A.22) such that

$$l_{\text{osc}}^{-1} = \sqrt{\Delta_{\gamma\gamma}^2/4 + \Delta_{\gamma g}^2} = \frac{1}{2} \sqrt{\omega^2(1 - \mu)^2 + 2\kappa\bar{B}^2}. \quad (\text{A.29})$$

Note that (A.28) is suitable for a propagation distance up to the coherence scale, $l \lesssim l_{\text{cor}}$, so that the uniformity of magnetic field can be assumed. For a larger distance $D > l_{\text{cor}}$, the total conversion probability can be approximated by averaging out the sinusoidal part in equation (A.28) as 1/2 to yield

$$\mathcal{P}_{g \rightarrow \gamma}(D) \simeq \frac{1}{4} \kappa (\bar{B} l_{\text{osc}})^2 \left(\frac{D}{l_{\text{cor}}} \right), \quad (\text{A.30})$$

which leads to the expression quoted as equation (2.1)⁴,

$$\mathcal{P}_{g \rightarrow \gamma} \approx 5.87 \times 10^{-29} \left(\frac{B}{1 \mu\text{G}} \right)^2 \left(\frac{\omega}{100 \text{ GHz}} \right)^2 \left(\frac{10^{-3} \text{ cm}^{-3}}{n_e} \right)^2 \left(\frac{D}{1 \text{ Mpc}} \right) \left(\frac{10 \text{ kpc}}{l_{\text{cor}}} \right). \quad (\text{A.31})$$

B Modelling baryonic physics inside galaxy clusters

We briefly elaborate on the BCM that yields the gas profile ρ_{gas} and electron number density n_e used for the kSZ effect calculations in Section 3.1. We employed a baryon model, initially presented in Ref. [188], and further refined in subsequent works [126, 127], to capture and characterise the processes inside clusters. The matter inside the galaxy clusters consists of collisionless dark matter (clm), gas and the central galaxy matter (cga). In BCM, the total matter (ρ_{dmb}) is given as,

$$\rho_{\text{dmb}}(r) = \rho_{\text{clm}}(r) + \rho_{\text{gas}}(r) + \rho_{\text{cga}}(r), \quad (\text{B.1})$$

where the gas profile is given by

$$\rho_{\text{gas}} \propto \frac{\Omega_b / \Omega_m - f_{\text{star}} / M_{\text{vir}}}{[1 + 10(r/r_{\text{vir}})]^{\beta(M_{\text{vir}})} [1 + r/(\theta_{\text{ej}} r_{\text{vir}})]^{[\delta - \beta(M_{\text{vir}})]/\gamma}}, \quad (\text{B.2})$$

with β being a mass-dependent slope, f_{cga} the stellar-to-halo fractions of the central galaxy, and f_{star} the total stellar content. These quantities are parameterised as,

$$\beta(M_{\text{vir}}) = \frac{3(M_{\text{vir}}/M_c)^\mu}{1 + (M_{\text{vir}}/M_c)^\mu}, \quad f_i(M_{\text{vir}}) = \frac{M_i}{M_{\text{vir}}} = 0.055 \left(\frac{M_S}{M_{\text{vir}}} \right)^{\eta_i}, \quad (\text{B.3})$$

where $i \in \{\text{cga}, \text{star}\}$, $M_S = 2 \times 10^{11} M_\odot / h$ and the power indices are $\eta_{\text{star}} = \eta$ and $\eta_{\text{cga}} = \eta + \eta_\delta$. Here $\Omega_b / \Omega_{\text{mat}}$ is the baryon fraction, r_{vir} and M_{vir} are the virial radius and mass. Note that in the large-cluster limit, equation (B.2) approaches the truncated Navarro-Frenk-White (NFW) profile, i.e., $\lim_{M_{\text{vir}} \gg M_c} \beta = 3$. In essence, the electron number density depends on a 7-parameter model with five gas parameters $\boldsymbol{\theta}_{\text{gas}} \equiv (\log M_c, \mu, \theta_{\text{ej}}, \gamma, \delta)$, and two stellar parameters $\boldsymbol{\theta}_{\text{star}} \equiv (\eta, \eta_\delta)$. In this study, we fixed the model with $\boldsymbol{\theta}_{\text{gas}} = (13.4, 0.3, 4, 2, 7)$ and $\boldsymbol{\theta}_{\text{star}} = (0.32, 0.28)$, which is within the 95% credible region of the constraints in Ref. [123].

C Full posterior distribution of the SKA forecast study

To forecast the constraining capability of SKA, we use a Bayesian framework that provides the posterior distribution $\mathcal{P}(\boldsymbol{\theta}|\mathbf{d})$ quantifying the probability of model parameters $\boldsymbol{\theta}$ given data vector \mathbf{d} . This quantity is given as follows,

$$\mathcal{P}(\boldsymbol{\theta}|\mathbf{d}) \propto \mathcal{L}(\mathbf{d}|\boldsymbol{\theta}) \pi(\boldsymbol{\theta}), \quad (\text{C.1})$$

⁴Note that computing the numerical values requires restoring the correct dimensions in several expressions, e.g., $\omega_{\text{pl}}^2 \rightarrow \omega_{\text{pl}}^2 / \varepsilon_0$ from equation (A.8) onward, $\kappa \rightarrow \kappa / \mu_0$ from equation (A.28) onward, and $\omega^2 \rightarrow \omega^2 / c^2$ in equation (A.29).

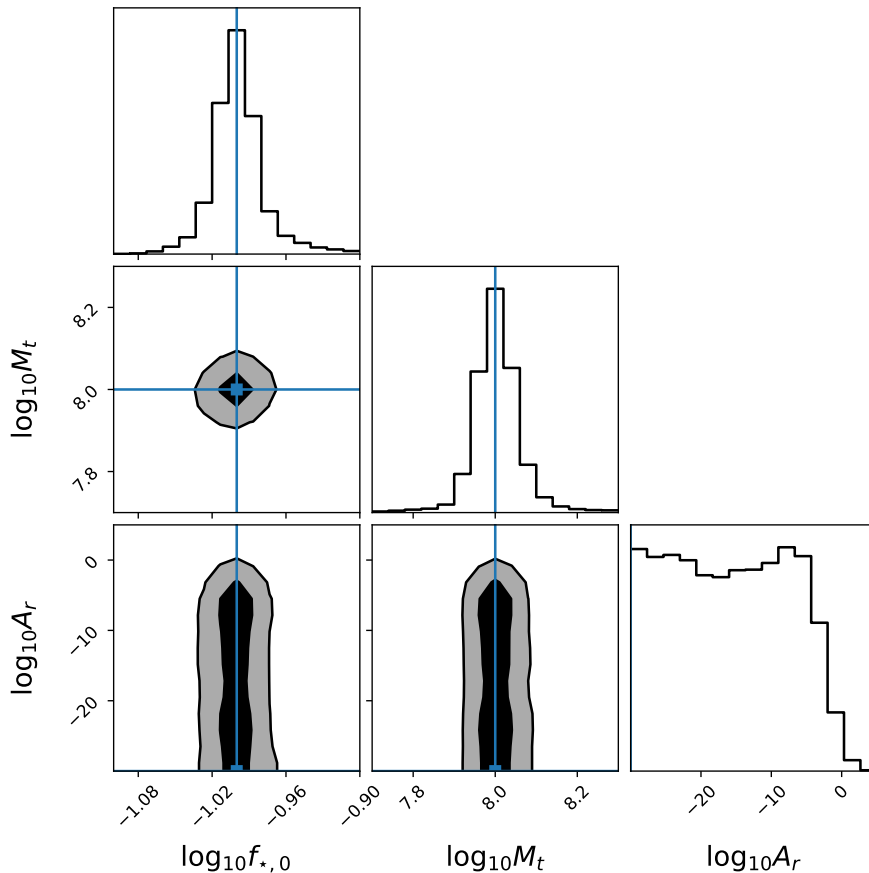


Figure 4: Posterior distribution on the model parameters expected from upcoming SKA-Low measurements with 1000 hour observing time. The assumed parameter values for the mock observation is shown with blue lines. The dark and light contours represent the 68% and 95% confidence level. We see that this measurement will not only constrain the astrophysical processes, it will provide strong upper limits on the excess radio background ($\log_{10}A_r$) that can be translated into constraints on the HFGWs.

where $\mathcal{L}(\mathbf{d}|\boldsymbol{\theta})$ and $\pi(\boldsymbol{\theta})$ are the likelihood and prior distribution respectively. We assume a Gaussian likelihood that is given in equation (21) of Ref. [79]. This likelihood incorporates the impact of both the cosmic variance and system noise expected from 1000 hour with SKA observation.

We use an MCMC sampler implemented in the publicly available `emcee` package⁵ [189] for exploring model parameter space. Below we describe these model parameter along with the assumed prior range for each of them.

1. $f_{*,0}$: The amplitude of the star formation rate in the dark matter haloes hosting photon sources during these early times. The number of photons emitted is proportional to the stellar mass. Therefore we can control the amount of emitted photons with this parameter. We consider a flat prior between 0.01 and 1 in log-space, which is consistent

⁵The package can be found at <https://emcee.readthedocs.io/en/stable/>.

with models required to interpret the ultraviolet luminosity function measurements [e.g. 190, 191]. We assume $f_{*,0} = 0.1$ for producing the mock observation.

2. M_t : The minimum dark matter mass that can sustain star formation. We consider a flat prior between 3.2×10^6 and $3.2 \times 10^9 M_\odot/h$ in log-space. We assume $M_t = 10^8 M_\odot/h$, which is close to the threshold that can sustain source formation due to molecular cooling [192, 193].
3. A_r : The parameter describing the magnitude of excess radio background corresponding to the 21-cm signal. In order to explore interesting values shown in Figure 2, we consider a flat prior between -30 and 30 in log-space. We produced the mock observation assuming absence of excess radio background that is quantified as $A_r = 10^{-30}$.

As the goal of this study is to study the constraints in the HFGWs that depends only on A_r , we have chosen a simple two parameter astrophysical model to describe the photon sources during cosmic dawn. In Figure 4, we show the full corner plot⁶ for the posterior distribution from the MCMC run. We find that the ground truth for the two astrophysical parameters are predicted correctly at both the 68% and 95% confidence level. We estimated an upper limit on the excess radio background with $A_r \lesssim 10^{-9}$ at 68% confidence level from the 1D marginalised posterior distribution.

References

- [1] LIGO SCIENTIFIC, VIRGO collaboration, *GWTC-1: A Gravitational-Wave Transient Catalog of Compact Binary Mergers Observed by LIGO and Virgo during the First and Second Observing Runs*, *Phys. Rev. X* **9** (2019) 031040 [1811.12907].
- [2] LIGO SCIENTIFIC, VIRGO collaboration, *GWTC-2: Compact Binary Coalescences Observed by LIGO and Virgo During the First Half of the Third Observing Run*, *Phys. Rev. X* **11** (2021) 021053 [2010.14527].
- [3] LIGO SCIENTIFIC, VIRGO, KAGRA collaboration, *GWTC-3: Compact Binary Coalescences Observed by LIGO and Virgo During the Second Part of the Third Observing Run*, 2111.03606.
- [4] NANOGrav collaboration, *The NANOGrav 15 yr Data Set: Evidence for a Gravitational-wave Background*, *Astrophys. J. Lett.* **951** (2023) L8 [2306.16213].
- [5] EPTA collaboration, *The second data release from the European Pulsar Timing Array III. Search for gravitational wave signals*, 2306.16214.
- [6] D.J. Reardon et al., *Search for an Isotropic Gravitational-wave Background with the Parkes Pulsar Timing Array*, *Astrophys. J. Lett.* **951** (2023) L6 [2306.16215].
- [7] H. Xu et al., *Searching for the Nano-Hertz Stochastic Gravitational Wave Background with the Chinese Pulsar Timing Array Data Release I*, *Res. Astron. Astrophys.* **23** (2023) 075024 [2306.16216].
- [8] BICEP2, PLANCK collaboration, *Joint Analysis of BICEP2/KeckArray and Planck Data*, *Phys. Rev. Lett.* **114** (2015) 101301 [1502.00612].
- [9] BICEP2, KECK ARRAY collaboration, *BICEP2 / Keck Array x: Constraints on Primordial Gravitational Waves using Planck, WMAP, and New BICEP2/Keck Observations through the 2015 Season*, *Phys. Rev. Lett.* **121** (2018) 221301 [1810.05216].

⁶The plot is produced using the `corner` package [194] that can be found at <https://corner.readthedocs.io/en/latest/>.

- [10] PLANCK collaboration, *Planck 2018 results. VI. Cosmological parameters*, *Astron. Astrophys.* **641** (2020) A6 [[1807.06209](#)].
- [11] T. Namikawa, S. Saga, D. Yamauchi and A. Taruya, *CMB Constraints on the Stochastic Gravitational-Wave Background at Mpc scales*, *Phys. Rev. D* **100** (2019) 021303 [[1904.02115](#)].
- [12] LISA collaboration, *Laser Interferometer Space Antenna*, [1702.00786](#).
- [13] J.E. Kim, H.P. Nilles and M. Peloso, *Completing natural inflation*, *JCAP* **01** (2005) 005 [[hep-ph/0409138](#)].
- [14] M. Peloso and C. Unal, *Trajectories with suppressed tensor-to-scalar ratio in Aligned Natural Inflation*, *JCAP* **06** (2015) 040 [[1504.02784](#)].
- [15] V. Domcke, M. Pieroni and P. Binétruy, *Primordial gravitational waves for universality classes of pseudoscalar inflation*, *JCAP* **06** (2016) 031 [[1603.01287](#)].
- [16] J. Garcia-Bellido, M. Peloso and C. Unal, *Gravitational waves at interferometer scales and primordial black holes in axion inflation*, *JCAP* **12** (2016) 031 [[1610.03763](#)].
- [17] D.G. Figueroa and F. Torrenti, *Gravitational wave production from preheating: parameter dependence*, *JCAP* **10** (2017) 057 [[1707.04533](#)].
- [18] S. Kanemura and K. Kaneta, *Gravitational Waves from Particle Decays during Reheating*, [2310.12023](#).
- [19] C. Caprini and D.G. Figueroa, *Cosmological Backgrounds of Gravitational Waves*, *Class. Quant. Grav.* **35** (2018) 163001 [[1801.04268](#)].
- [20] N. Aggarwal et al., *Challenges and opportunities of gravitational-wave searches at MHz to GHz frequencies*, *Living Rev. Rel.* **24** (2021) 4 [[2011.12414](#)].
- [21] R. Brito, V. Cardoso and P. Pani, *Superradiance: New Frontiers in Black Hole Physics*, *Lect. Notes Phys.* **906** (2015) pp.1 [[1501.06570](#)].
- [22] A.D. Dolgov and D. Ejlli, *Relic gravitational waves from light primordial black holes*, *Phys. Rev. D* **84** (2011) 024028 [[1105.2303](#)].
- [23] T. Fujita, M. Kawasaki, K. Harigaya and R. Matsuda, *Baryon asymmetry, dark matter, and density perturbation from primordial black holes*, *Phys. Rev. D* **89** (2014) 103501 [[1401.1909](#)].
- [24] A. Ejlli, D. Ejlli, A.M. Cruise, G. Pisano and H. Grote, *Upper limits on the amplitude of ultra-high-frequency gravitational waves from graviton to photon conversion*, *Eur. Phys. J. C* **79** (2019) 1032 [[1908.00232](#)].
- [25] N. Herman, A. Füzfa, L. Lehoucq and S. Clesse, *Detecting planetary-mass primordial black holes with resonant electromagnetic gravitational-wave detectors*, *Phys. Rev. D* **104** (2021) 023524 [[2012.12189](#)].
- [26] G. Franciolini, A. Maharana and F. Muia, *Hunt for light primordial black hole dark matter with ultrahigh-frequency gravitational waves*, *Phys. Rev. D* **106** (2022) 103520 [[2205.02153](#)].
- [27] M. Oncins, *Constraints on PBH as dark matter from observations: a review*, [2205.14722](#).
- [28] T.C. Gehrman, B. Shams Es Haghi, K. Sinha and T. Xu, *Baryogenesis, primordial black holes and MHz–GHz gravitational waves*, *JCAP* **02** (2023) 062 [[2211.08431](#)].
- [29] T.C. Gehrman, B. Shams Es Haghi, K. Sinha and T. Xu, *The primordial black holes that disappeared: connections to dark matter and MHz–GHz gravitational Waves*, *JCAP* **10** (2023) 001 [[2304.09194](#)].
- [30] P.G. Macedo and A.H. Nelson, *PROPAGATION OF GRAVITATIONAL WAVES IN A MAGNETIZED PLASMA*, *Phys. Rev. D* **28** (1983) 2382.
- [31] G. Raffelt and L. Stodolsky, *Mixing of the Photon with Low Mass Particles*, *Phys. Rev. D* **37** (1988) 1237.

- [32] A.M. Cruise, *The potential for very high-frequency gravitational wave detection*, *Class. Quant. Grav.* **29** (2012) 095003.
- [33] A.D. Dolgov and D. Ejlli, *Conversion of relic gravitational waves into photons in cosmological magnetic fields*, *JCAP* **12** (2012) 003 [[1211.0500](#)].
- [34] D. Ejlli and V.R. Thandlam, *Graviton-photon mixing*, *Phys. Rev. D* **99** (2019) 044022 [[1807.00171](#)].
- [35] D. Ejlli, *Graviton-photon mixing. Exact solution in a constant magnetic field*, *JHEP* **06** (2020) 029 [[2004.02714](#)].
- [36] J.A.R. Cembranos, M.G. Ortiz and P. Martín-Moruno, *Graviton-photon oscillation in a cosmic background for a general theory of gravity*, [2302.08186](#).
- [37] M.E. Gertsenshtein, *Wave resonance of light and gravitational waves*, *Soviet Journal of Experimental and Theoretical Physics* **15** (1962) 84.
- [38] D. Boccaletti, V. Sabbata, P. Fortini and C. Gualdi, *Conversion of photons into gravitons and vice versa in a static electromagnetic field*, *Nuovo Cimento B Serie* **70** (1970) 129.
- [39] D.J. Stevenson, *Planetary Magnetic Fields: Achievements and Prospects*, *Space Sci. Rev.* **152** (2010) 651.
- [40] G. Schubert and K.M. Soderlund, *Planetary magnetic fields: Observations and models*, *Physics of the Earth and Planetary Interiors* **187** (2011) 92.
- [41] A. Reiners, *Observations of Cool-Star Magnetic Fields*, *Living Reviews in Solar Physics* **9** (2012) 1 [[1203.0241](#)].
- [42] R. Beck, *Galactic and extragalactic magnetic fields*, *Space Sci. Rev.* **99** (2001) 243 [[astro-ph/0012402](#)].
- [43] F. Govoni and L. Feretti, *Magnetic Fields in Clusters of Galaxies*, *International Journal of Modern Physics D* **13** (2004) 1549 [[astro-ph/0410182](#)].
- [44] T. Liu, J. Ren and C. Zhang, *Detecting High-Frequency Gravitational Waves in Planetary Magnetosphere*, [2305.01832](#).
- [45] A. Dolgov and K. Postnov, *Electromagnetic Radiation Accompanying Gravitational Waves from Black Hole Binaries*, *JCAP* **09** (2017) 018 [[1706.05519](#)].
- [46] C.-J. Feng, A. Guo, Z.-M. Xie and M. Li, *Photons generated by gravitational waves in the near-zone of a neutron star*, *Nucl. Phys. B* **985** (2022) 116029 [[2207.14517](#)].
- [47] A. Kushwaha, S. Malik and S. Shankaranarayanan, *Gertsenshtein-Zel'dovich effect explains the origin of Fast Radio Bursts*, [2202.00032](#).
- [48] A. Ito, K. Kohri and K. Nakayama, *Probing high frequency gravitational waves with pulsars*, [2305.13984](#).
- [49] A. Kushwaha, S. Malik and S. Shankaranarayanan, *Fast radio bursts signal high-frequency gravitational waves*, *Int. J. Mod. Phys. D* **32** (2023) 2342010 [[2311.11150](#)].
- [50] S. Ramazanov, R. Samanta, G. Trenkler and F.R. Urban, *Shimmering gravitons in the gamma-ray sky*, *JCAP* **06** (2023) 019 [[2304.11222](#)].
- [51] M.S. Pshirkov and D. Baskaran, *Limits on High-Frequency Gravitational Wave Background from its interplay with Large Scale Magnetic Fields*, *Phys. Rev. D* **80** (2009) 042002 [[0903.4160](#)].
- [52] V. Domcke and C. Garcia-Cely, *Potential of radio telescopes as high-frequency gravitational wave detectors*, *Phys. Rev. Lett.* **126** (2021) 021104 [[2006.01161](#)].
- [53] A.M. Cruise, *An electromagnetic detector for very-high-frequency gravitational waves*, *Class. Quant. Grav.* **17** (2000) 2525.

- [54] L.P. Grishchuk, *Electromagnetic generators and detectors of gravitational waves*, in *1st Conference on High Frequency Gravitational Waves*, 6, 2003 [[gr-qc/0306013](#)].
- [55] A.M. Cruise and R.M.J. Ingley, *A prototype gravitational wave detector for 100-MHz*, *Class. Quant. Grav.* **23** (2006) 6185.
- [56] A. Füzfa, *Electromagnetic Gravitational Waves Antennas for Directional Emission and Reception*, [1702.06052](#).
- [57] A. Berlin, D. Blas, R. Tito D’Agnolo, S.A.R. Ellis, R. Harnik, Y. Kahn et al., *Detecting high-frequency gravitational waves with microwave cavities*, *Phys. Rev. D* **105** (2022) 116011 [[2112.11465](#)].
- [58] V. Domcke, C. Garcia-Cely and N.L. Rodd, *Novel Search for High-Frequency Gravitational Waves with Low-Mass Axion Haloscopes*, *Phys. Rev. Lett.* **129** (2022) 041101 [[2202.00695](#)].
- [59] V. Domcke, C. Garcia-Cely, S.M. Lee and N.L. Rodd, *Symmetries and Selection Rules: Optimising Axion Haloscopes for Gravitational Wave Searches*, [2306.03125](#).
- [60] A. Berlin, D. Blas, R. Tito D’Agnolo, S.A.R. Ellis, R. Harnik, Y. Kahn et al., *MAGO 2.0: Electromagnetic Cavities as Mechanical Bars for Gravitational Waves*, [2303.01518](#).
- [61] G. Vacalis, G. Marocco, J. Bamber, R. Bingham and G. Gregori, *Detection of high-frequency gravitational waves using high-energy pulsed lasers*, *Class. Quant. Grav.* **40** (2023) 155006 [[2301.08163](#)].
- [62] K. Schmieden and M. Schott, *The Global Network of Cavities to Search for Gravitational Waves (GravNet): A novel scheme to hunt gravitational waves signatures from the early universe*, [2308.11497](#).
- [63] T. Bringmann, V. Domcke, E. Fuchs and J. Kopp, *High-Frequency Gravitational Wave Detection via Optical Frequency Modulation*, [2304.10579](#).
- [64] J.E. Carlstrom, G.P. Holder and E.D. Reese, *Cosmology with the sunyaev-zel’dovich effect*, *Annual Review of Astronomy and Astrophysics* **40** (2002) 643.
- [65] ATACAMA COSMOLOGY TELESCOPE collaboration, *Atacama Cosmology Telescope: Combined kinematic and thermal Sunyaev-Zel’dovich measurements from BOSS CMASS and LOWZ halos*, *Phys. Rev. D* **103** (2021) 063513 [[2009.05557](#)].
- [66] S. Amodeo et al., *Atacama Cosmology Telescope: Modeling the gas thermodynamics in BOSS CMASS galaxies from kinematic and thermal Sunyaev-Zel’dovich measurements*, *Phys. Rev. D* **103** (2021) 063514 [[2009.05558](#)].
- [67] J.R. Pritchard and A. Loeb, *21 cm cosmology in the 21st century*, *Reports on Progress in Physics* **75** (2012) 086901.
- [68] C. Feng and G. Holder, *Enhanced global signal of neutral hydrogen due to excess radiation at cosmic dawn*, *The Astrophysical Journal Letters* **858** (2018) L17.
- [69] A. Fialkov and R. Barkana, *Signature of Excess Radio Background in the 21-cm Global Signal and Power Spectrum*, *Mon. Not. Roy. Astron. Soc.* **486** (2019) 1763 [[1902.02438](#)].
- [70] J.D. Bowman, A.E.E. Rogers, R.A. Monsalve, T.J. Mozdzen and N. Mahesh, *An absorption profile centred at 78 megahertz in the sky-averaged spectrum*, *Nature* **555** (2018) 67 [[1810.05912](#)].
- [71] A. Ewall-Wice, T.-C. Chang, J. Lazio, O. Doré, M. Seiffert and R. Monsalve, *Modeling the radio background from the first black holes at cosmic dawn: implications for the 21 cm absorption amplitude*, *The Astrophysical Journal* **868** (2018) 63.
- [72] I. Reis, A. Fialkov and R. Barkana, *High-redshift radio galaxies: a potential new source of 21-cm fluctuations*, *Monthly Notices of the Royal Astronomical Society* **499** (2020) 5993.

- [73] F.G. Mertens, M. Mevius, L.V. Koopmans, A. Offringa, G. Mellema, S. Zaroubi et al., *Improved upper limits on the 21 cm signal power spectrum of neutral hydrogen at $z \approx 9.1$ from lofar*, *Monthly Notices of the Royal Astronomical Society* **493** (2020) 1662.
- [74] C.M. Trott, C. Jordan, S. Midgley, N. Barry, B. Greig, B. Pindor et al., *Deep multiredshift limits on epoch of reionization 21 cm power spectra from four seasons of munchison widefield array observations*, *Monthly Notices of the Royal Astronomical Society* **493** (2020) 4711.
- [75] G. Mellema, L.V.E. Koopmans, F.A. Abdalla, G. Bernardi, B. Ciardi, S. Daiboo et al., *Reionization and the Cosmic Dawn with the Square Kilometre Array*, *Experimental Astronomy* **36** (2013) 235 [[1210.0197](#)].
- [76] B. Greig and A. Mesinger, *21cmc: an mcmc analysis tool enabling astrophysical parameter studies of the cosmic 21 cm signal*, *Monthly Notices of the Royal Astronomical Society* **449** (2015) 4246.
- [77] C.A. Watkinson, B. Greig and A. Mesinger, *Epoch of reionization parameter estimation with the 21-cm bispectrum*, *Monthly Notices of the Royal Astronomical Society* **510** (2022) 3838.
- [78] I. Georgiev, A. Gorce and G. Mellema, *Constraining cosmic reionization by combining the kinetic Sunyaev–Zel’dovich and the 21 cm power spectra*, *Mon. Not. Roy. Astron. Soc.* **528** (2024) 7218 [[2312.04259](#)].
- [79] S.K. Giri and A. Schneider, *Imprints of fermionic and bosonic mixed dark matter on the 21-cm signal at cosmic dawn*, *Physical Review D* **105** (2022) 083011.
- [80] A. Schneider, T. Schaeffer and S.K. Giri, *Cosmological forecast of the 21-cm power spectrum using the halo model of reionization*, [2302.06626](#).
- [81] T.E. Clarke, *Faraday Rotation Observations of Magnetic Fields in Galaxy Clusters*, *Journal of Korean Astronomical Society* **37** (2004) 337 [[astro-ph/0412268](#)].
- [82] M. Murgia, F. Govoni, L. Feretti, G. Giovannini, D. Dallacasa, R. Fanti et al., *Magnetic fields and Faraday rotation in clusters of galaxies*, *Astron. Astrophys.* **424** (2004) 429 [[astro-ph/0406225](#)].
- [83] C. Vogt and T.A. Ensslin, *A Bayesian view on Faraday rotation maps - Seeing the magnetic power spectra in galaxy clusters*, *Astron. Astrophys.* **434** (2005) 67 [[astro-ph/0501211](#)].
- [84] F. Govoni, M. Murgia, V. Vacca, F. Loi, M. Girardi, F. Gastaldello et al., *Sardinia Radio Telescope observations of Abell 194. The intra-cluster magnetic field power spectrum*, *A&A* **603** (2017) A122 [[1703.08688](#)].
- [85] R. Fusco-Femiano, D. Dal Fiume, M. Orlandini, G. Brunetti, L. Feretti and G. Giovannini, *Hard X-Ray Emission from the Galaxy Cluster A3667*, *Astrophys. J. Lett.* **552** (2001) L97 [[astro-ph/0105049](#)].
- [86] R. Fusco-Femiano, M. Orlandini, G. Brunetti, L. Feretti, G. Giovannini, P. Grandi et al., *Confirmation of Nonthermal Hard X-Ray Excess in the Coma Cluster from Two Epoch Observations*, *Astrophys. J. Lett.* **602** (2004) L73 [[astro-ph/0312625](#)].
- [87] M. Brüggen, A. Bykov, D. Ryu and H. Röttgering, *Magnetic Fields, Relativistic Particles, and Shock Waves in Cluster Outskirts*, *Space Sci. Rev.* **166** (2012) 187 [[1107.5223](#)].
- [88] R.J. van Weeren, F. de Gasperin, H. Akamatsu, M. Brüggen, L. Feretti, H. Kang et al., *Diffuse Radio Emission from Galaxy Clusters*, *Space Sci. Rev.* **215** (2019) 16 [[1901.04496](#)].
- [89] B.F.C. Cooper and R.M. Price, *Faraday Rotation Effects associated with the Radio Source Centaurus A*, *Nature* **196** (1962) 761.
- [90] B.J. Burn, *On the depolarization of discrete radio sources by Faraday dispersion*, *MNRAS* **133** (1966) 67.

- [91] M. Brüggen, T.H. Reiprich, E. Bulbul, B.S. Koribalski, H. Andernach, L. Rudnick et al., *Radio observations of the merging galaxy cluster system Abell 3391-Abell 3395*, *A&A* **647** (2021) A3 [2012.08775].
- [92] V. Missaglia, M. Murgia, F. Massaro, A. Paggi, A. Jimenez-Gallardo, W.R. Forman et al., *High-frequency Radio Imaging of 3CR 403.1 with the Sardinia Radio Telescope*, *Astrophys. J.* **936** (2022) 10 [2207.13711].
- [93] T. Vernstrom, B.M. Gaensler, L. Rudnick and H. Andernach, *Differences in Faraday Rotation between Adjacent Extragalactic Radio Sources as a Probe of Cosmic Magnetic Fields*, *Astrophys. J.* **878** (2019) 92 [1905.02410].
- [94] S.P. O’Sullivan, M. Brüggen, F. Vazza, E. Carretti, N.T. Locatelli, C. Stuardi et al., *New constraints on the magnetization of the cosmic web using LOFAR Faraday rotation observations*, *MNRAS* **495** (2020) 2607 [2002.06924].
- [95] F. Govoni, E. Orrù, A. Bonafede, M. Iacobelli, R. Paladino, F. Vazza et al., *A radio ridge connecting two galaxy clusters in a filament of the cosmic web*, *Science* **364** (2019) 981 [1906.07584].
- [96] A. Botteon, R. Cassano, D. Eckert, G. Brunetti, D. Dallacasa, T.W. Shimwell et al., *Particle acceleration in a nearby galaxy cluster pair: the role of cluster dynamics*, *A&A* **630** (2019) A77 [1908.07527].
- [97] F. Marinacci, M. Vogelsberger, P. Mocz and R. Pakmor, *The large-scale properties of simulated cosmological magnetic fields*, *Mon. Not. Roy. Astron. Soc.* **453** (2015) 3999 [1506.00005].
- [98] F. Vazza, G. Brunetti, M. Brüggen and A. Bonafede, *Resolved magnetic dynamo action in the simulated intracluster medium*, *MNRAS* **474** (2018) 1672 [1711.02673].
- [99] P. Domínguez-Fernández, F. Vazza, M. Brüggen and G. Brunetti, *Dynamical evolution of magnetic fields in the intracluster medium*, *MNRAS* **486** (2019) 623 [1903.11052].
- [100] U.P. Steinwandel, L.M. Boess, K. Dolag and H. Lesch, *On the small scale turbulent dynamo in the intracluster medium: A comparison to dynamo theory*, *arXiv e-prints* (2021) arXiv:2108.07822 [2108.07822].
- [101] S. Mchedlidze, P. Domínguez-Fernández, X. Du, W. Schmidt, A. Brandenburg, J. Niemeyer et al., *Inflationary and Phase-transitional Primordial Magnetic Fields in Galaxy Clusters*, *Astrophys. J.* **944** (2023) 100 [2210.10183].
- [102] J. Donnert, F. Vazza, M. Brüggen and J. ZuHone, *Magnetic Field Amplification in Galaxy Clusters and Its Simulation*, *SSR* **214** (2018) 122 [1810.09783].
- [103] F. Govoni, M. Murgia, L. Feretti, G. Giovannini, K. Dolag and G.B. Taylor, *The intracluster magnetic field power spectrum in Abell 2255*, *A&A* **460** (2006) 425 [astro-ph/0608433].
- [104] A. Neronov and I. Vovk, *Evidence for Strong Extragalactic Magnetic Fields from Fermi Observations of TeV Blazars*, *Science* **328** (2010) 73 [1006.3504].
- [105] M.S. Pshirkov, P.G. Tinyakov and F.R. Urban, *New Limits on Extragalactic Magnetic Fields from Rotation Measures*, *Phys. Rev. L* **116** (2016) 191302 [1504.06546].
- [106] K.E. Kunze and M.A. Vázquez-Mozo, *Constraints on hidden photons from current and future observations of CMB spectral distortions*, *JCAP* **12** (2015) 028 [1507.02614].
- [107] A.D. Dolgov, L.A. Panasencko and V.A. Bochko, *Graviton to photon conversion in curved space-time and external magnetic field*, **2310.19838**.
- [108] R.R. Lindner, A.J. Baker, J.P. Hughes, N. Battaglia, N. Gupta, K. Knowles et al., *The Radio Relics and Halo of El Gordo, a Massive $z = 0.870$ Cluster Merger*, *Astrophys. J.* **786** (2014) 49 [1310.6786].

- [109] G. Di Gennaro, R.J. van Weeren, G. Brunetti, R. Cassano, M. Brüggen, M. Hoeft et al., *Fast magnetic field amplification in distant galaxy clusters*, *Nature Astronomy* **5** (2021) 268 [2011.01628].
- [110] G. Di Gennaro, M. Brüggen, R.J. van Weeren, A. Simionescu, G. Brunetti, R. Cassano et al., *The diffuse radio emission in the high-redshift cluster PSZ2 G091.83+26.11: Total intensity and polarisation analysis with Very Large Array 1-4 GHz observations*, *A&A* **675** (2023) A51 [2304.05893].
- [111] F. Aharonian, J. Aschersleben, M. Backes, V.B. Martins, R. Batzofin, Y. Becherini et al., *Constraints on the Intergalactic Magnetic Field Using Fermi-LAT and H.E.S.S. Blazar Observations*, *Astrophys. J. Lett.* **950** (2023) L16 [2306.05132].
- [112] M.S. Turner and L.M. Widrow, *Inflation-produced, large-scale magnetic fields*, *Phys. Rev. D* **37** (1988) 2743.
- [113] B. Ratra, *Cosmological “Seed” Magnetic Field from Inflation*, *Astrophys. J. Lett.* **391** (1992) L1.
- [114] S. Kanno, J. Soda and M.-a. Watanabe, *Cosmological magnetic fields from inflation and backreaction*, *J. Cosmol. Astropart. Phys.* **2009** (2009) 009 [0908.3509].
- [115] R. Emami, H. Firouzjahi and M.S. Movahed, *Inflation from charged scalar and primordial magnetic fields?*, *Phys. Rev. D* **81** (2010) 083526 [0908.4161].
- [116] T. Fujita and S. Mukohyama, *Universal upper limit on inflation energy scale from cosmic magnetic field*, *J. Cosmol. Astropart. Phys.* **2012** (2012) 034 [1205.5031].
- [117] C.J. Hogan, *Magnetohydrodynamic Effects of a First-Order Cosmological Phase Transition*, *Phys. Rev. L* **51** (1983) 1488.
- [118] J.M. Quashnock, A. Loeb and D.N. Spergel, *Magnetic Field Generation during the Cosmological QCD Phase Transition*, *Astrophys. J. Lett.* **344** (1989) L49.
- [119] G. Baym, D. Bödeker and L. McLerran, *Magnetic fields produced by phase transition bubbles in the electroweak phase transition*, *Phys. Rev. D* **53** (1996) 662 [hep-ph/9507429].
- [120] B. Cheng, A.V. Olinto, D.N. Schramm and J.W. Truran, *Constraints on the strength of primordial magnetic fields from big bang nucleosynthesis reexamined*, *Phys. Rev. D* **54** (1996) 4714 [astro-ph/9606163].
- [121] K. Subramanian, *The origin, evolution and signatures of primordial magnetic fields*, *RPPh* **79** (2016) 076901 [1504.02311].
- [122] T. Vernstrom, G. Heald, F. Vazza, T.J. Galvin, J. West, N. Locatelli et al., *Discovery of magnetic fields along stacked cosmic filaments as revealed by radio and X-ray emission*, *Mon. Not. Roy. Astron. Soc.* **505** (2021) 4178 [2101.09331].
- [123] A. Schneider, S.K. Giri, S. Amodeo and A. Refregier, *Constraining baryonic feedback and cosmology with weak-lensing, X-ray, and kinematic Sunyaev–Zeldovich observations*, *Mon. Not. Roy. Astron. Soc.* **514** (2022) 3802 [2110.02228].
- [124] I.G. McCarthy, J. Schaye, S. Bird and A.M.C. Le Brun, *The bahamas project: calibrated hydrodynamical simulations for large-scale structure cosmology*, *Monthly Notices of the Royal Astronomical Society* (2016) stw2792.
- [125] J. Braspenning, J. Schaye, M. Schaller, I.G. McCarthy, S.T. Kay, J.C. Helly et al., *The flamingo project: Galaxy clusters in comparison to x-ray observations*, *arXiv preprint arXiv:2312.08277* (2023) .
- [126] A. Schneider, R. Teyssier, J. Stadel, N.E. Chisari, A.M. Le Brun, A. Amara et al., *Quantifying baryon effects on the matter power spectrum and the weak lensing shear correlation*, *Journal of Cosmology and Astroparticle Physics* **2019** (2019) 020.

- [127] S.K. Giri and A. Schneider, *Emulation of baryonic effects on the matter power spectrum and constraints from galaxy cluster data*, *Journal of Cosmology and Astroparticle Physics* **2021** (2021) 046.
- [128] D. Fixsen, A. Kogut, S. Levin, M. Limon, P. Lubin, P. Mirel et al., *Arcade 2 measurement of the absolute sky brightness at 3–90 ghz*, *The Astrophysical Journal* **734** (2011) 5.
- [129] J. Dowell and G.B. Taylor, *The radio background below 100 mhz*, *The Astrophysical Journal Letters* **858** (2018) L9.
- [130] R.H. Cyburt, B.D. Fields, K.A. Olive and T.-H. Yeh, *Big Bang Nucleosynthesis: 2015*, *Rev. Mod. Phys.* **88** (2016) 015004 [[1505.01076](#)].
- [131] L. Pagano, L. Salvati and A. Melchiorri, *New constraints on primordial gravitational waves from Planck 2015*, *Phys. Lett. B* **760** (2016) 823 [[1508.02393](#)].
- [132] R. Mondal et al., *Tight constraints on the excess radio background at $z = 9.1$ from LOFAR*, *Mon. Not. Roy. Astron. Soc.* **498** (2020) 4178 [[2004.00678](#)].
- [133] R. Ghara, S.K. Giri, B. Ciardi, G. Mellema and S. Zaroubi, *Constraining the state of the intergalactic medium during the Epoch of Reionization using MWA 21-cm signal observations*, *Mon. Not. Roy. Astron. Soc.* **503** (2021) 4551 [[2103.07483](#)].
- [134] Y. Mao, M. Tegmark, M. McQuinn, M. Zaldarriaga and O. Zahn, *How accurately can 21 cm tomography constrain cosmology?*, *Physical Review D* **78** (2008) 023529.
- [135] N.S. Kern, A. Liu, A.R. Parsons, A. Mesinger and B. Greig, *Emulating simulations of cosmic dawn for 21 cm power spectrum constraints on cosmology, reionization, and x-ray heating*, *The Astrophysical Journal* **848** (2017) 23.
- [136] HERA collaboration, *Improved Constraints on the 21 cm EoR Power Spectrum and the X-Ray Heating of the IGM with HERA Phase I Observations*, *Astrophys. J.* **945** (2023) 124 [[2210.04912](#)].
- [137] B. Cyr, J. Chluba and S.K. Acharya, *A cosmic string solution to the radio synchrotron background*, *arXiv preprint arXiv:2308.03512* (2023) .
- [138] D.J. Fixsen, A. Kogut, S. Levin, M. Limon, P. Lubin, P. Mirel et al., *ARCADE 2 Measurement of the Absolute Sky Brightness at 3-90 GHz*, *APJ* **734** (2011) 5 [[0901.0555](#)].
- [139] A. Schneider, S.K. Giri and J. Mirocha, *Halo model approach for the 21-cm power spectrum at cosmic dawn*, *Physical Review D* **103** (2021) 083025.
- [140] S.K. Giri, G. Mellema and H. Jensen, *Tools21cm: A python package to analyse the large-scale 21-cm signal from the epoch of reionization and cosmic dawn*, *Journal of Open Source Software* **5** (2020) 2363.
- [141] S.K. Giri, G. Mellema and R. Ghara, *Optimal identification of $h ii$ regions during reionization in 21-cm observations*, *Monthly Notices of the Royal Astronomical Society* **479** (2018) 5596.
- [142] J.C. Pober, A. Liu, J.S. Dillon, J.E. Aguirre, J.D. Bowman, R.F. Bradley et al., *What next-generation 21 cm power spectrum measurements can teach us about the epoch of reionization*, *The Astrophysical Journal* **782** (2014) 66.
- [143] S.K. Giri, G. Mellema, T. Aldheimer, K.L. Dixon and I.T. Iliev, *Neutral island statistics during reionization from 21-cm tomography*, *Monthly Notices of the Royal Astronomical Society* **489** (2019) 1590.
- [144] H.E. Ross, S.K. Giri, G. Mellema, K.L. Dixon, R. Ghara and I.T. Iliev, *Redshift-space distortions in simulations of the 21-cm signal from the cosmic dawn*, *Monthly Notices of the Royal Astronomical Society* **506** (2021) 3717.
- [145] I. Georgiev, G. Mellema, S.K. Giri and R. Mondal, *The large-scale 21-cm power spectrum from reionization*, *Monthly Notices of the Royal Astronomical Society* **513** (2022) 5109.

- [146] M. Mevius, F. Mertens, L. Koopmans, A. Offringa, S. Yatawatta, M. Brentjens et al., *A numerical study of 21-cm signal suppression and noise increase in direction-dependent calibration of lofar data*, *Monthly Notices of the Royal Astronomical Society* **509** (2022) 3693.
- [147] H. Gan, F. Mertens, L. Koopmans, A. Offringa, M. Mevius, V. Pandey et al., *Assessing the impact of two independent direction-dependent calibration algorithms on the lofar 21 cm signal power spectrum-and applications to an observation of a field flanking the north celestial pole*, *Astronomy & Astrophysics* **669** (2023) A20.
- [148] S.K. Giri, A. D’Aloisio, G. Mellema, E. Komatsu, R. Ghara and S. Majumdar, *Position-dependent power spectra of the 21-cm signal from the epoch of reionization*, *Journal of Cosmology and Astroparticle Physics* **2019** (2019) 058.
- [149] C.A. Watkinson, S.K. Giri, H.E. Ross, K.L. Dixon, I.T. Iliev, G. Mellema et al., *The 21-cm bispectrum as a probe of non-gaussianities due to x-ray heating*, *Monthly Notices of the Royal Astronomical Society* **482** (2019) 2653.
- [150] M. Bianco, S.K. Giri, I.T. Iliev and G. Mellema, *Deep learning approach for identification of h ii regions during reionization in 21-cm observations*, *Monthly Notices of the Royal Astronomical Society* **505** (2021) 3982.
- [151] M. Bianco, S. Giri, D. Prelogović, T. Chen, F.G. Mertens, E. Tolley et al., *Deep learning approach for identification of hii regions during reionization in 21-cm observations-ii. foreground contamination*, *arXiv preprint arXiv:2304.02661* (2023) .
- [152] J. Chluba et al., *New horizons in cosmology with spectral distortions of the cosmic microwave background*, *Exper. Astron.* **51** (2021) 1515 [[1909.01593](#)].
- [153] A. Kogut, M.H. Abitbol, J. Chluba, J. Delabrouille, D. Fixsen, J.C. Hill et al., *CMB Spectral Distortions: Status and Prospects*, [1907.13195](#).
- [154] A. Kogut et al., *The Primordial Inflation Explorer (PIXIE): A Nulling Polarimeter for Cosmic Microwave Background Observations*, *JCAP* **07** (2011) 025 [[1105.2044](#)].
- [155] K. Basu et al., *A space mission to map the entire observable universe using the CMB as a backlight: Voyage 2050 science white paper*, *Exper. Astron.* **51** (2021) 1555 [[1909.01592](#)].
- [156] A. Ito, K. Kohri and K. Nakayama, *Gravitational wave search through electromagnetic telescopes*, [2309.14765](#).
- [157] M. Chianese, P. Di Bari, K. Farrag and R. Samanta, *Probing relic neutrino radiative decays with 21 cm cosmology*, *Phys. Lett. B* **790** (2019) 64 [[1805.11717](#)].
- [158] P.S.B. Dev, P. Di Bari, I. Martínez-Soler and R. Roshan, *Relic neutrino decay solution to the excess radio background*, [2312.03082](#).
- [159] A. Caputo, M. Regis, M. Taoso and S.J. Witte, *Detecting the Stimulated Decay of Axions at RadioFrequencies*, *JCAP* **03** (2019) 027 [[1811.08436](#)].
- [160] N. Fornengo, R. Lineros, M. Regis and M. Taoso, *Possibility of a Dark Matter Interpretation for the Excess in Isotropic Radio Emission Reported by ARCADE*, *Phys. Rev. Lett.* **107** (2011) 271302 [[1108.0569](#)].
- [161] A. Caputo, H. Liu, S. Mishra-Sharma, M. Pospelov and J.T. Ruderman, *Radio excess from stimulated dark matter decay*, *Phys. Rev. D* **107** (2023) 123033 [[2206.07713](#)].
- [162] R.D. Peccei and H.R. Quinn, *CP Conservation in the Presence of Instantons*, *Phys. Rev. Lett.* **38** (1977) 1440.
- [163] R.D. Peccei and H.R. Quinn, *Constraints Imposed by CP Conservation in the Presence of Instantons*, *Phys. Rev. D* **16** (1977) 1791.
- [164] S. Weinberg, *A New Light Boson?*, *Phys. Rev. Lett.* **40** (1978) 223.

- [165] F. Wilczek, *Problem of Strong P and T Invariance in the Presence of Instantons*, *Phys. Rev. Lett.* **40** (1978) 279.
- [166] D.J.E. Marsh, *Axions and ALPs: a very short introduction*, in *13th Patras Workshop on Axions, WIMPs and WISPs*, pp. 59–74, 2018, DOI [1712.03018].
- [167] J. Preskill, M.B. Wise and F. Wilczek, *Cosmology of the Invisible Axion*, *Phys. Lett. B* **120** (1983) 127.
- [168] L.F. Abbott and P. Sikivie, *A Cosmological Bound on the Invisible Axion*, *Phys. Lett. B* **120** (1983) 133.
- [169] M. Dine and W. Fischler, *The Not So Harmless Axion*, *Phys. Lett. B* **120** (1983) 137.
- [170] L.D. Duffy and K. van Bibber, *Axions as Dark Matter Particles*, *New J. Phys.* **11** (2009) 105008 [0904.3346].
- [171] C.B. Adams et al., *Axion Dark Matter*, in *Snowmass 2021*, 3, 2022 [2203.14923].
- [172] E.G.M. Ferreira, *Ultra-light dark matter*, *Astron. Astrophys. Rev.* **29** (2021) 7 [2005.03254].
- [173] M. Johnston-Hollitt, F. Govoni, R. Beck, S. Dehghan, L. Pratley, T. Akahori et al., *Using SKA Rotation Measures to Reveal the Mysteries of the Magnetised Universe*, in *Advancing Astrophysics with the Square Kilometre Array (AASKA14)*, p. 92, Apr., 2015, DOI [1506.00808].
- [174] G. Tobar, S.K. Manikandan, T. Beitel and I. Pikovski, *Detecting single gravitons with quantum sensing*, [2308.15440](#).
- [175] Y. Kahn, J. Schütte-Engel and T. Trickle, *Searching for High Frequency Gravitational Waves with Phonons*, [2311.17147](#).
- [176] A. Arvanitaki and A.A. Geraci, *Detecting high-frequency gravitational waves with optically-levitated sensors*, *Phys. Rev. Lett.* **110** (2013) 071105 [1207.5320].
- [177] N. Aggarwal, G.P. Winstone, M. Teo, M. Baryakhtar, S.L. Larson, V. Kalogera et al., *Searching for New Physics with a Levitated-Sensor-Based Gravitational-Wave Detector*, *Phys. Rev. Lett.* **128** (2022) 111101 [2010.13157].
- [178] C.M. Caves, *MICROWAVE CAVITY GRAVITATIONAL RADIATION DETECTORS*, *Phys. Lett. B* **80** (1979) 323.
- [179] C.E. Reece, P.J. Reiner and A.C. Melissinos, *OBSERVATION OF $4 \times 10^{*-17}$ -CM HARMONIC DISPLACEMENT USING A 10-GHZ SUPERCONDUCTING PARAMETRIC CONVERTER*, *Phys. Lett. A* **104** (1984) 341.
- [180] C.E. Reece, P.J. Reiner and A.C. Melissinos, *A Detector for High Frequency Gravitational Effects Based on Parametric Conversion at 10 GHz*, *eConf* **C8206282** (1982) 394.
- [181] F. Pegoraro, L.A. Radicati, P. Bernard and E. Picasso, *Electromagnetic Detector for Gravitational Waves*, *Phys. Lett. A* **68** (1978) 165.
- [182] M. Goryachev and M.E. Tobar, *Gravitational Wave Detection with High Frequency Phonon Trapping Acoustic Cavities*, *Phys. Rev. D* **90** (2014) 102005 [1410.2334].
- [183] A. Ito, T. Ikeda, K. Miuchi and J. Soda, *Probing GHz gravitational waves with graviton–magnon resonance*, *Eur. Phys. J. C* **80** (2020) 179 [1903.04843].
- [184] F. Villaescusa-Navarro, S. Genel, E. Castorina, A. Obuljen, D.N. Spergel, L. Hernquist et al., *Ingredients for 21 cm intensity mapping*, *The Astrophysical Journal* **866** (2018) 135.
- [185] T. Fujita, K. Kamada and Y. Nakai, *Gravitational Waves from Primordial Magnetic Fields via Photon-Graviton Conversion*, *Phys. Rev. D* **102** (2020) 103501 [2002.07548].
- [186] W. Heisenberg and H. Euler, *Consequences of Dirac’s theory of positrons*, *Z. Phys.* **98** (1936) 714 [physics/0605038].

- [187] J. Schwinger, *On gauge invariance and vacuum polarization*, *Phys. Rev.* **82** (1951) 664.
- [188] A. Schneider and R. Teyssier, *A new method to quantify the effects of baryons on the matter power spectrum*, *Journal of Cosmology and Astroparticle Physics* **2015** (2015) 049.
- [189] D. Foreman-Mackey, D.W. Hogg, D. Lang and J. Goodman, *emcee: the mcmc hammer*, *Publications of the Astronomical Society of the Pacific* **125** (2013) 306.
- [190] G. Sun, C.-A. Faucher-Giguère, C.C. Hayward, X. Shen, A. Wetzel and R.K. Cochrane, *Bursty star formation naturally explains the abundance of bright galaxies at cosmic dawn*, *The Astrophysical Journal Letters* **955** (2023) L35.
- [191] P. Dayal and S.K. Giri, *Warm dark matter constraints from the just*, *Monthly Notices of the Royal Astronomical Society* **528** (2024) 2784.
- [192] M. Tegmark, J. Silk, M.J. Rees, A. Blanchard, T. Abel and F. Palla, *How small were the first cosmological objects?*, *The Astrophysical Journal* **474** (1997) 1.
- [193] O. Nebrin, S.K. Giri and G. Mellema, *Starbursts in low-mass haloes at cosmic dawn. i. the critical halo mass for star formation*, *Monthly Notices of the Royal Astronomical Society* (2023) stad1852.
- [194] D. Foreman-Mackey, *corner.py: Scatterplot matrices in python*, *The Journal of Open Source Software* **1** (2016) 24.